

Advances in Detection and Error Correction for Coherent Optical Communications: Regular, Irregular, and Spatially Coupled LDPC Code Designs

Laurent Schmalen*, Stephan ten Brink†, and Andreas Leven*

1 Introduction

Forward error correction (FEC) in optical communications has been first demonstrated in 1988 [1]. Since then, coding technology has evolved significantly. This pertains not only to the codes but also to encoder and decoder architectures. Modern high-speed optical communication systems require high-performing FEC engines that support throughputs of 100 GBit/s or multiples thereof, that have low power consumption, that realize *net coding gains* (NCGs) close to the theoretical limits at a target *bit error rate* (BER) of below 10^{-15} , and that are preferably adapted to the peculiarities of the optical channel.

Forward error correction coding is based on deterministically adding redundant bits to a source information bit sequence. After transmission over a noisy channel, a decoding system tries to exploit the redundant information for fully recovering the source information. Several methods for generating the redundant bit sequence from the source information bits are known. Transmission systems with 100 GBit/s and 400 GBit/s today typically use one of two coding schemes to generate the redundant information: *Block-Turbo Codes* (BTCs) or *Low-Density Parity-Check* (LDPC) codes. In coherent systems, so-called soft information is usually readily available and can be used in high performing systems within a soft-decision decoder architecture. Soft-decision information means that no binary 0/1 decision is made before entering the forward error correction decoder. Instead, the (quantized) samples are used together with their statistics to get improved estimates of the original bit sequence. This chapter will focus on soft-decision decoding of LDPC codes and the evolving spatially coupled LDPC codes.

* L. Schmalen and A. Leven are with Nokia Bell Labs, Lorenzstr. 10, 70435 Stuttgart, Germany. E-mail: {first.last}@nokia-bell-labs.com

† S. ten Brink is with the University of Stuttgart, Institute of Telecommunications, Pfaffenwaldring 47, 70569 Stuttgart, Germany.

This is the version of the following article: “Advances in Detection and Error Correction for Coherent Optical Communications: Regular, Irregular, and Spatially Coupled LDPC Code Designs”, which appeared as Chapter 3 in the book *Enabling Technologies for High Spectral-efficiency Coherent Optical Communication Networks* edited by X. Zhou and C. Xie, which has been published in final form at DOI:10.1002/9781119078289 (ISBN 9781118714768 (print) and ISBN 9781119078289 (online)). This article may be used for non-commercial purposes in accordance with Wiley Terms and Conditions for Self-Archiving.

In coherent optical communications, the signal received after carrier recovery may be affected by different distortions than those that commonly occur in wireless communications. For instance, the signal at the input of the signal space demapper may be affected by phase slips (also called *cycle slips* [2]), with a probability depending on the non-linear phase noise introduced by the optical transmission link [3]. The phase slips are *not* an effect of the physical waveform channel but, rather, an artifact of coarse blind phase recovery algorithms with massive parallelization at the initial digital signal processing (DSP) receiver steps [4]. If such a phase slip is ignored, error propagation will occur at the receiver and all data following the phase slip cannot be properly recovered. Several approaches to mitigate phase slips have been proposed. Of these, the most common is differential coding, rendering a phase slip into a single error event. In order to alleviate the penalty caused by differential coding, iterative decoding between an FEC decoder and a differential decoder can be beneficial [5]. This solution leads however to an increased receiver complexity, as several executions of a soft-input soft-output differential decoder (usually based on the BCJR algorithm¹) have to be carried out.

In this chapter, we first show how the use of differential coding and the presence of phase slips in the transmission channel affect the total achievable information rates and capacity of a system. By means of the commonly used *Quadrature Phase-Shift Keying* (QPSK) modulation, we show that the use of differential coding *does not decrease the capacity*, i.e., the total amount of reliably conveyable information over the channel remains the same. It is a common misconception that the use of differential coding introduces an unavoidable “differential loss”. This *perceived* differential loss is rather a consequence of simplified differential detection and decoding at the receiver. Afterwards, we show how capacity-approaching coding schemes based on LDPC and spatially coupled LDPC codes can be constructed by combining iterative demodulation and decoding. For this, we first show how to modify the differential decoder to account for phase slips and then how to use this modified differential decoder to construct good LDPC codes. This construction method can serve as a blueprint to construct good and practical LDPC codes for other applications with iterative detection, such as higher order modulation formats with non-square constellations [7], multi-dimensional optimized modulation formats [8], turbo equalization to mitigate ISI (e.g., due to nonlinearities) [9, 10] and many more. Finally, we introduce the class of *spatially coupled* (SC)-LDPC codes, which are a specialization of LDPC codes with some outstanding properties and which can be decoded with a very simple windowed decoder. We show that the universal behavior of spatially coupled codes makes them an ideal candidate for iterative differential demodulation/detection and decoding.

This chapter is structured as follows: In Sec. 2 we formally introduce the notation, system model and differential coding. We highlight some pitfalls that one may encounter when phase slips occur on the equivalent channel. We propose a modified differential decoder that is necessary to construct a capacity-approaching system with differential coding. In Sec. 3, we introduce LDPC codes and iterative detection. We highlight several possibilities of realizing the interface between the LDPC decoder and the detector and give design

¹termed after the initial letters of its inventors Bahl, Cocke, Jelinek and Raviv [6].

guidelines for finding good degree distributions of the LDPC code. We show that with iterative detection and LDPC codes, the differential loss can be recovered to a great extent. Finally, in Sec. 4, we introduce SC-LDPC codes and show how a very simple construction can be used to realize codes that outperform LDPC codes while having similar decoding complexity.

2 Differential Coding for Optical Communications

In this section, we describe and study the effect of differential coding on coherent optical communication systems and especially on the maximum conveyable information rate (the so-called *capacity*). We assume a simple, yet accurate channel model based on *additive white Gaussian noise* (AWGN) and random phase slips. We start by giving a rigorous description of higher-order modulation schemes frequently used in coherent communications and then introduce in Sec. 2.2 the channel model taking into account phase slips which are due to imperfect phase estimation in the coherent receiver. We will then introduce differential coding and show how the differential decoder has to be modified in order to properly take into account phase slips. We show that differential coding as such does not limit the capacity of a communication system, provided that an adequate receiver is used.

2.1 Higher-Order Modulation Formats

In this section, the interplay of coding and modulation will be discussed in detail. We only take on an IQ-perspective of digital modulation, representing digital modulation symbols as complex numbers. The sequence of complex numbers (where I denotes the real part and Q the imaginary part) is then used to generate the actual waveform (taking into account pulse shaping and eventually electronic pre-distortion), i.e., to drive the optical modulators generating the I and Q component. For a thorough overview of coding and modulation in the context of coherent communications, we refer the interested reader to [11, 12].

When talking about digital modulation, especially in the context of coded modulation, we are mostly interested in the *mapping function*, which is that part of the modulator that assigns (complex) modulation symbols to bit patterns. We introduce in what follows the notation necessary for describing the mapping function. Let q denote the number of bits that are assigned to one complex modulation symbol $y \in \mathbb{C}$, and let $\mathbf{b} = (b_1, b_2, \dots, b_q) \in \mathbb{F}_2^q$ be a binary q -tuple with $\mathbb{F}_2 = \{0, 1\}$ denoting the field of binary numbers. The one-to-one modulation mapping function $y = \phi(\mathbf{b})$ maps the q -tuple \mathbf{b} to the (complex) modulation symbol $y \in \mathbb{C}$, where y is chosen from the set of $Q = 2^q$ modulation symbols $\mathcal{M} = \{M_0, M_1, \dots, M_{Q-1}\}$. The set \mathcal{M} is also commonly referred to as *constellation*. The mapping function is illustrated in Fig. 1. In this chapter, we only consider one-to-one mappings. One such mapping is $\phi_{\text{Nat}}(\mathbf{b}) = \phi_{\text{Nat}}(b_1, b_2, \dots, b_q) = M_{(b_1 b_2 \dots b_q)_{10}}$, where $(b_1 b_2 \dots b_q)_{10}$ denotes the decimal expansion of the binary q -digit number $b_1 b_2 \dots b_q$.

In the context of differential coding of higher-order modulation formats, it is advantageous if the constellation \mathcal{M} fulfills certain properties. One such property is the *rotational invariance* of the constellation.

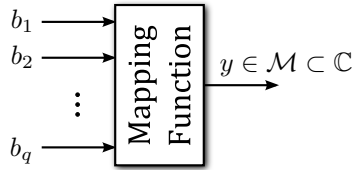


Figure 1: Mapping of a group of q bits (b_1, b_2, \dots, b_q) to a modulation symbol $y \in \mathbb{C}$

Definition 1 (Rotational Invariance of Constellation) We say that a constellation $\mathcal{M} = \{M_0, M_1, \dots, M_{Q-1}\}$ exhibits a V -fold rotational invariance if we recover the original constellation \mathcal{M} after rotating each modulation symbol M_i by an amount $\frac{2\pi}{V}k$, $\forall k \in \{1, \dots, V\}$ in the complex plane. Formally, we say that a constellation exhibits a V -fold rotational invariance if (with $\iota = \sqrt{-1}$)

$$\{M_i \cdot e^{i\frac{2\pi}{V}k} : M_i \in \mathcal{M}\} = \mathcal{M} \quad \text{for all } k \in \{1, \dots, V\}.$$

Example 2.1 Consider the two constellations with 8 and 16 points shown in Fig. 2. The rectangular 8-QAM (quadrature amplitude modulation) constellation of Fig. 2-(a) has a $V = 2$ two-fold rotational invariance as any rotation of the constellation by π leads again to the same constellation. The 16-QAM constellation shown in Fig. 2-(b) exhibits a $V = 4$ four-fold rotational invariance as any rotation of the constellation by $\frac{\pi}{2}$ leads again to the same constellation.

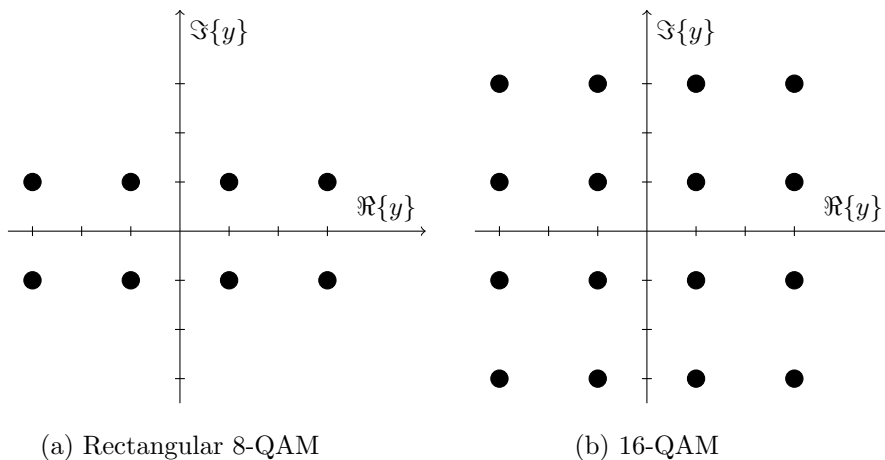


Figure 2: Two common higher order constellations: (a) Rectangular 8-QAM with $Q = 8$ and $V = 2$, and (b) 16-QAM with $Q = 16$ and $V = 4$

Before introducing differential coding and modulation, we first describe the channel model including phase slips.

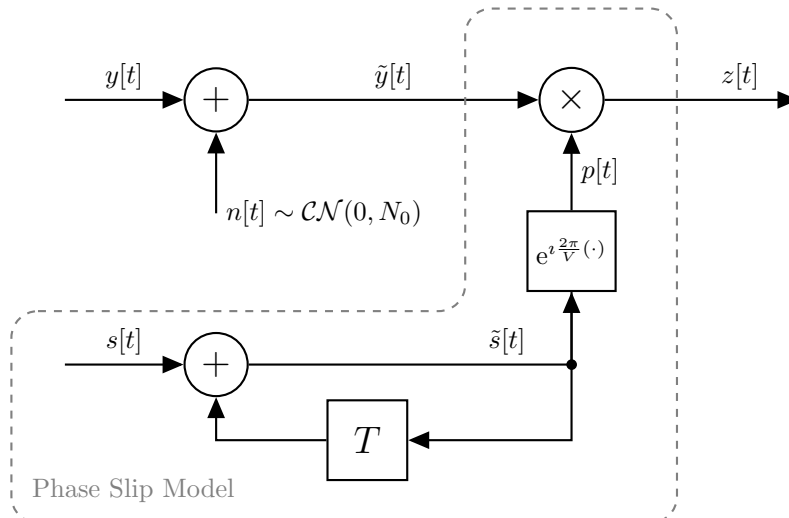


Figure 3: AWGN channel model with phase slips

2.2 The Phase Slip Channel Model

In coherent receivers for high-speed optical communications, it is usually not feasible to employ decision-directed blind phase recovery [4] so that usually, feed-forward phase recovery algorithms have to be employed. Feed-Forward carrier recovery algorithms exploit the rotational invariance of the constellation to remove the modulation prior to estimating the phase. However, due to the necessary phase unwrapping algorithm in the feed-forward phase estimator, a phenomenon called *phase slip* occurs². These are mostly due to coarse blind phase recovery algorithms with massive parallelization including preliminary hard decisions and phase unwrapping at the initial *digital signal processing* (DSP) receiver steps [4].

Figure 3 displays the phase-slip channel model we employ in the following. The channel input is a complex modulation symbol $y[t] \in \mathcal{M} \subset \mathcal{C}$. The first noise contribution is complex-valued AWGN. In the field of coding and in the broad body of literature on forward error correction, the terms E_s/N_0 and E_b/N_0 are frequently used to characterize AWGN channels. Therein, $E_s = \mathbf{E}\{|y|^2\}$ denotes the energy per modulation symbol³. The noise $n[t] = n_I[t] + \imath n_Q[t]$ (where $\imath = \sqrt{-1}$) is characterized by the two-sided noise power spectral density $N_0 = 2\sigma_n^2$ where σ_n^2 is the variance of both noise components $n_I[t]$ and $n_Q[t]$, i.e., $\sigma_n^2 = \mathbf{var}(n_I[t]) = \mathbf{var}(n_Q[t])$. The received symbol $z[t]$ in our model is obtained by $z[t] = (y[t] + n[t]) \cdot p[t]$, where $p[t]$ describes the phase slips. Phase slips and $p[t]$ will be discussed in detail below.

Frequently, especially for comparing different coding schemes, E_b/N_0 is used instead of

²Sometimes, phase slips are also denoted as *cycle slips*, however, we employ the term phase slip in this chapter.

³Note that in this chapter we use lower case letters to denote random variables as well as their realizations to avoid confusion, unless it is not clear from the context.

E_s/N_0 . Herein, E_b denotes the energy per *information bit* whereas E_s denotes the energy per *transmit symbol*. For example, if a code of rate $r = 4/5$, corresponding to an overhead of $\Omega = \frac{1}{r} - 1 \doteq 25\%$, is used, the ratio of n code bits versus k information bits amounts to $n/k = 5/4 = 1.25$, i.e., $1.25 = 1/r$ code bits are transmitted for each information bit. Thereof, q code bits are assigned to one modulation symbol $y[t]$. This means that if the modulation symbols will be transmitted each with energy E_s , the amount of energy conveyed by each information bit amounts to

$$E_s = E_b \cdot q \cdot r \quad \Leftrightarrow \quad E_b = \frac{E_s}{q \cdot r}.$$

As E_b is normalized to the information bits of the transmission system, it allows us to immediately evaluate the *net coding gain* (NCG). The NCG is frequently used to assess the performance of a coding scheme and is defined as the difference (in dB) of required E_b/N_0 values between coded and uncoded transmission for a given output BER. Note that the NCG takes into account the coding rate r and the number of bits assigned to each modulation symbol, which are included in E_b .

In optical communications, the *optical signal-to-noise ratio* (OSNR) is also frequently employed. The OSNR is the signal-to-noise ratio measured in a reference optical bandwidth, where frequently a bandwidth B_{ref} of 12.5 GHz is used corresponding to 0.1 nm wavelength. The OSNR relates to the E_s/N_0 and E_b/N_0 as

$$\text{OSNR} \Big|_{\text{dB}} = \frac{E_s}{N_0} \Big|_{\text{dB}} + 10 \log_{10} \frac{R_S}{B_{\text{ref}}} = \frac{E_b}{N_0} \Big|_{\text{dB}} + 10 \log_{10} \frac{q \cdot r \cdot R_S}{B_{\text{ref}}}$$

where B_{ref} is the previously introduced reference bandwidth, R_S corresponds to the symbol rate of the transmission, r is the aforementioned rate of the code with $r = k/n$ and q corresponds to the number of bits mapped to each modulation symbol.

Returning to the description of the channel model of Fig. 3, we see that the noisy signal $\tilde{y}[t]$ additionally undergoes a potential phase rotation yielding $z[t]$. If the constellation shows a V -fold rotational invariance with V even (which is the case for most of the practically relevant constellations), we introduce the following probabilistic phase slip model

$$\begin{aligned} P(s[t] = \pm 1) &= \xi \\ P(s[t] = \pm 2) &= \xi^2 \\ &\vdots \\ P\left(s[t] = \pm \frac{V}{2}\right) &= \xi^{V/2} \end{aligned}$$

The probability that a phase slip occurs is thus

$$P_{\text{slip}} = 2 \sum_{i=1}^{V/2} \xi^i = 2 \left(\frac{1 - \xi^{V/2+1}}{1 - \xi} - 1 \right) = \frac{2\xi(1 - \xi^{V/2})}{1 - \xi}. \quad (1)$$

For a given phase slip probability, which may be obtained from measurements [2], and which depends on the non-linear phase noise introduced by the optical transmission link and variance of the additive Gaussian noise due to amplification, we obtain the value ξ by solving (1) for ξ . For the practically most important cases with $V = 2$, and $V = 4$, we get

$$\xi = \begin{cases} \frac{P_{\text{slip}}}{2} & \text{if } V = 2 \\ \frac{\sqrt{2P_{\text{slip}}+1}}{2} - \frac{1}{2} & \text{if } V = 4. \end{cases} \quad (2)$$

Experimental measurements [13] suggest that the phase slip probability depends on the equivalent bit error rate before the FEC decoder. Such a dependency was also suggested in [3]. We may thus model P_{slip} empirically as

$$P_{\text{slip}} = \begin{cases} \min\left(1, \frac{\gamma}{2} \operatorname{erfc}\left(\sqrt{\frac{E_s}{N_0}}\right)\right), & \text{for BPSK} \\ \min\left(1, \frac{\gamma}{2} \operatorname{erfc}\left(\sqrt{\frac{E_s}{2N_0}}\right)\right), & \text{for QPSK} \end{cases} \quad (3)$$

where γ is the factor between slip rate and pre-FEC bit error rate for the equivalent BPSK channel. Given E_s/N_0 and γ , we can compute P_{slip} from (3) and subsequently ξ from (2) or (1). Using ξ , we can use a pseudo-random number generator to generate a sequence of $s[t]$ with the probability mass function defined above.

2.3 Differential Coding and Decoding

Several approaches to mitigate phase slips have been proposed in the literature. Probably the most common is differential coding, rendering a phase slip into a single error event. In this section, we restrict ourselves for simplicity to constellations with a V -fold rotational invariance where $V = 2^v$, $v \in \mathbb{N}$, i.e., $V \in \{2, 4, 8, 16, \dots\}$.

We consider two different cases:

1. In the first case, we have $V = Q$. To each constellation point, we assign a state S_i , $i \in \{1, \dots, V\}$. An example of such a constellation is the widely used QPSK constellation with $V = 4$, which is shown in Fig. 4 together with its state assignment.

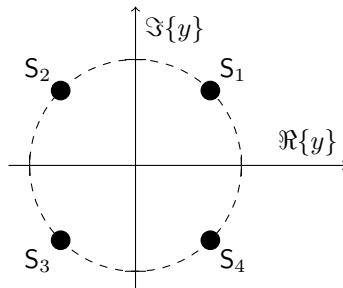


Figure 4: Example of a QPSK constellation with state assignment in rotational order

2. In the second case, we have $Q > V$. We restrict ourselves to the practical case with $Q = J \cdot V$, where J is an integer number. In this case, we employ differential coding as described in [14]: The constellation is divided into V disjoint regions such that these regions are preserved when rotating the constellation by $\pm \frac{2\pi}{V}$. We assign a state label S_i to each disjoint region. The regions are selected such that each region contains exactly $J = \frac{Q}{V} = 2^j$ constellation points and such that a rotation of the constellation by an angle $\kappa \cdot \frac{2\pi}{V}$, $\kappa \in \{0, \pm 1, \pm 2, \dots\}$ does neither change the regions nor the assignment of points to a region. For the constellation points within each region we employ a *rotationally invariant* bit mapping, which means that the bit mapping of points inside a region is not changed by a rotation of the constellation by an angle $\kappa \cdot \frac{2\pi}{V}$. The popular 16-QAM constellation is an example of such a constellation with $Q = 16$, $V = 4$ and $J = 4$. The state assignment and rotationally invariant mapping are exemplarily discussed in Example 2.2 and shown in Fig. 5.

Example 2.2 We consider the transmission of the popular 16-QAM constellation [15]. It can be easily verified that the 16-QAM constellation shows a $V = 4$ -fold rotational invariance. As shown in Fig. 5, we label the four quadrants of the complex plane by states S_1 , S_2 , S_3 , and S_4 . Inside the first quadrant S_1 , we employ a Gray labeling (also denoted by mapping) to assign the bits b_3 and b_4 to the four points. The mapping of the bits b_3 and b_4 in the three remaining quadrants is obtained by applying a rotational invariant mapping, i.e., by rotating the Gray mapping of S_1 by multiples of $\frac{\pi}{2}$. In this case, even by rotating the constellation by multiples of $\frac{\pi}{2}$, the bits b_3 and b_4 can always be recovered unambiguously.

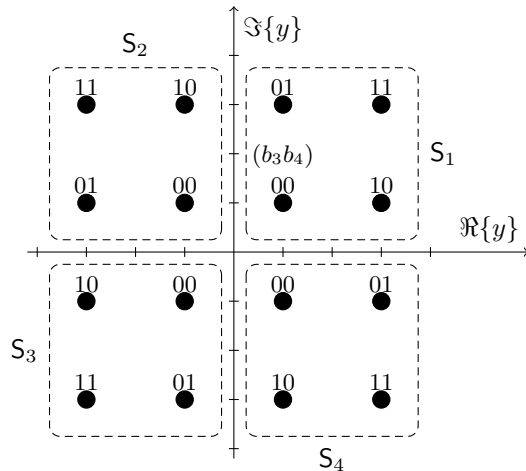


Figure 5: Differential coding for the 16-QAM constellation ($V = 4$) with rotational invariant bit mapping in each quadrant

We employ differential coding with $v = \log_2(V)$ bits to encode and reliably transmit the region, i.e., the state. Within each of these regions, exactly Q/V constellation points

are placed, to which a *rotationally invariant* bit mapping is assigned. This means that whenever the constellation is rotated by an angle that is a multiple of $\frac{2\pi}{V}$, the bit patterns assigned to constellation points within the region can still be uniquely identified. Note that we restrict ourselves to state-region assignments such that the rotation of a complete region gives another valid region, i.e., $\forall i \in \{1, \dots, V\}$, there exists a $j \in \{1, \dots, V\}$, such that

$$\left\{ z \cdot e^{i\kappa \frac{2\pi}{V}} : z \in S_i \right\} = S_j, \quad \forall \kappa \in \{0, \pm 1, \pm 2, \dots\}.$$

Note that this restriction does not impose any problems for practical systems as most of the practically relevant constellations can be described in this form. In what follows, we impose another, slightly more stringent condition on the states. We assume that the states S_i are assigned in what we denote as *rotational order*. Formally,

Definition 2 We define a sequence of states S_i , $i \in \{1, \dots, V\}$ that are assigned to a region of the complex plane, to be in rotational order, if and only if the following condition

$$\left\{ z \cdot e^{i\kappa \frac{2\pi}{V}} : z \in S_i \right\} = S_{((i+\kappa-1) \bmod V)+1}, \quad \forall \kappa \in \mathbb{N}$$

is fulfilled.

We can easily verify that the state assignments of the constellations given in Fig. 4 and Fig. 5 are in rotational order. Again, note that the restriction of the states to be in *rotational order* does not yet impose any major constraint, as we have not yet defined an encoding map. We group the V states into the set $\mathcal{S} := \{S_1, S_2, \dots, S_V\}$.

The main step in differential coding is to impose memory on the modulation. We assume that the transmission starts at time instant $t = 1$. We introduce the differential memory $\mathbf{d}_t^{[\text{mem}]} \in \mathcal{S}$ and set $\mathbf{d}_0^{[\text{mem}]} = S_1$. The differential encoder can be considered to be the function

$$f_{\text{diff}} : \mathcal{S} \times \mathbb{F}_2^v \rightarrow \mathcal{S}$$

$$(\mathbf{d}_{t-1}^{[\text{mem}]}, b_{t,1}, b_{t,2}, \dots, b_{t,v}) \mapsto f_{\text{diff}}(\mathbf{d}_{t-1}^{[\text{mem}]}, b_{t,1}, b_{t,2}, \dots, b_{t,v}) = \mathbf{d}_t^{[\text{mem}]},$$

which takes as input the bits $b_{t,1}, \dots, b_{t,v}$ and the differential memory $\mathbf{d}_{t-1}^{[\text{mem}]}$ and generates a new state that is saved in the differential memory $\mathbf{d}_t^{[\text{mem}]}$. This new state $\mathbf{d}_t^{[\text{mem}]}$ selects the symbol to be transmitted (if $V = Q$) or the region from which the symbol is selected using the bits $b_{t,v+1}, \dots, b_{t,q}$. Note that the differential function is not unique but depends on the assignment of bit patterns to state transitions. Consider the example of the QPSK constellation shown in Fig. 4. We can give two distinct differential encoding maps. The first differential encoding function is the *natural differential code*. The state transition diagram of the natural differential code is visualized in Fig. 6 and is also given in Tab. 1. The second encoding function, baptized *Gray differential code* is given in Tab. 2. Note that all other differential coding maps for the QPSK constellation can be transformed into one of these two forms by elementary transformations of the constellation and the state assignment.

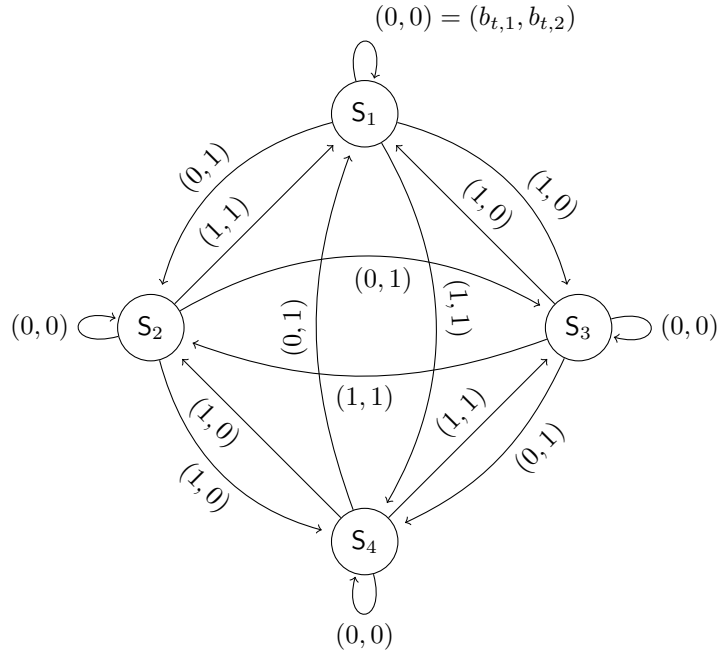


Figure 6: Differential encoding state transition diagram for the natural differential code. Arrow annotations are binary labels $(b_{t,1}, b_{t,2})$

Table 1: Differential encoding map f_{diff} for the natural differential code

$(b_{t,1}, b_{t,2})$	$d_{t-1}^{[\text{mem}]} = S_1$	$d_{t-1}^{[\text{mem}]} = S_2$	$d_{t-1}^{[\text{mem}]} = S_3$	$d_{t-1}^{[\text{mem}]} = S_4$
(0, 0)	S_1	S_2	S_3	S_4
(0, 1)	S_2	S_3	S_4	S_1
(1, 0)	S_3	S_4	S_1	S_2
(1, 1)	S_4	S_1	S_2	S_3

As the differential code can be understood as a Markov process, we can employ the BCJR algorithm [6] to carry out *bit-wise Maximum A Posteriori (MAP)* decoding of the differential code. For this, we may represent the differential code using a so-called trellis diagram. The trellis diagram is an “unrolled” version of the state diagram of Fig. 6. Figure 7 shows four segments of a trellis diagram for the natural differential encoding map. Four segments of the trellis diagram of the Gray differential encoding map are given in Fig. 8. The different input bit patterns (b_1, b_2) can be distinguished by different line styles (dashed, dotted, solid and “waved”).

If phase slips occur on the channel, memory is imposed on the channel as well. If this additional memory is not properly accounted for in the BCJR decoder of the differential code, the performance of the decoder will rapidly decrease, due to the decoder not being properly adapted to the channel model, as has been observed in [16]. We therefore need to

Table 2: Differential encoding map f_{diff} for the Gray differential code

$(b_{t,1}, b_{t,2})$	$d_{t-1}^{[\text{mem}]} = S_1$	$d_{t-1}^{[\text{mem}]} = S_2$	$d_{t-1}^{[\text{mem}]} = S_3$	$d_{t-1}^{[\text{mem}]} = S_4$
(0, 0)	S_1	S_2	S_3	S_4
(0, 1)	S_2	S_3	S_4	S_1
(1, 0)	S_4	S_1	S_2	S_3
(1, 1)	S_3	S_4	S_1	S_2

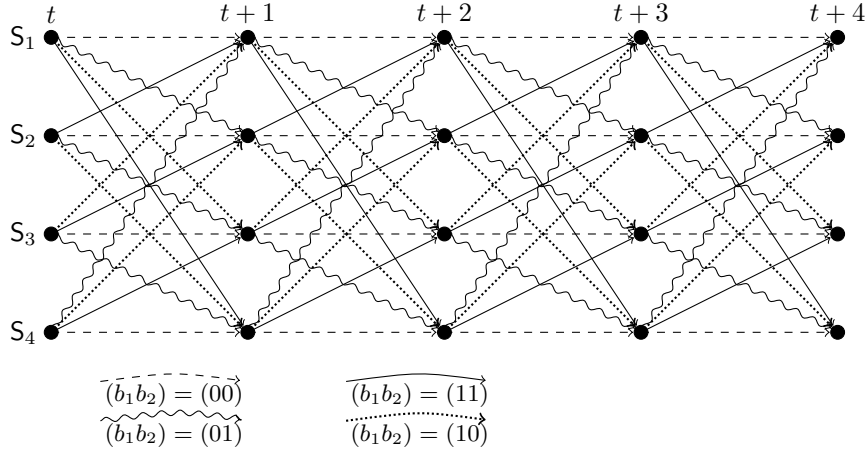


Figure 7: Trellis diagram for *natural* differential encoding of a constellation with $V = 4$ as given in Tab. 1

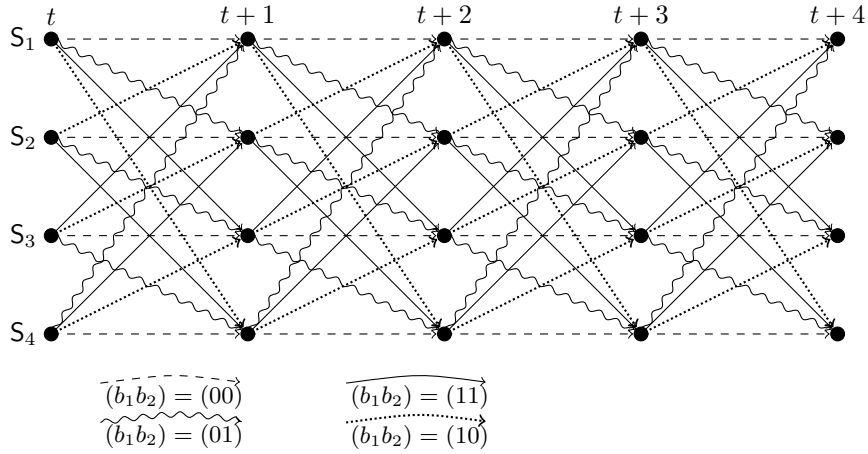


Figure 8: Trellis diagram for *Gray* differential encoding of a constellation with $V = 4$ as given in tab. 2

extend the trellis to properly *take into account the phase slips*. One such extension introduces additional states that correspond to the memory of the phase slip channel [17]. We introduce states $S_{i,\tilde{s}}$ where the second index \tilde{s} tracks the current phase slip state $\tilde{s}[t] \bmod 4$ (see Fig. 3), while the first index i is still responsible for describing the differential code. The occurrence of a phase slips ($s[t] \neq 0$) leads to a different $\tilde{s}[t]$. For the running example of a differential code for $V = 4$, we have no longer a trellis diagram (or a state transition diagram) with 4 states and $4 \cdot 4 = 16$ state transitions, but instead a trellis diagram with $4 \cdot 4 = 16$ states and $16 \cdot 16 = 256$ state transitions. One segment of this extended trellis diagram is shown in Fig. 9 for the Gray differential encoding map. In order to distinguish the additional state transitions corresponding to phase slips, we use grey scales. The original trellis is obtained by utilizing only those state transitions that correspond to $s[t] = 0$, which correspond to the black lines. The state transitions corresponding to $s[t] = 1$ and $s[t] = 3$ are given by grey lines while the state transitions corresponding to $s[t] = 2$ are given by light grey lines, as these have the lowest probability of occurrence.

As the trellis diagram of Fig. 9 may be challenging to implement, we seek for a way to reduce its complexity. By observing that the memory of the phase slip channel collapses with the memory of the differential encoder, we may get a more compact representation of the trellis and only need V states. This is possible as a phase slip does not introduce a new state, but only to a different state transition to one of the V existing states. In fact we have

$$d_t^{[\text{mem}]'} = S_{((i+s[t]-1) \bmod V)+1} \quad \text{with } S_i = d_t^{[\text{mem}]}$$

The state transitions are given exemplarily for the case of the Gray differential encoder in Tab. 3. This means that we can still use a trellis diagram with V states but have to insert additional state transitions taking into account all possible values of $s[t]$. Figure 10 shows the extended trellis diagram taking into account the possible slips, indicated by the slip value $s[t] \in \{0, 1, 2, 3\}$. Again, we use differential grey scales to represent the state transitions corresponding to different values of $s[t]$. The trellis diagram of Fig. 10 is a simplification of the extended trellis diagram with only $V = 4$ states (instead of 16) and $4 \cdot 16 = 64$ state transitions (instead of 256). Another approach to take into account phase slips into an extended trellis has been presented in [13].

2.4 Maximum a Posteriori Differential Decoding

In what follows, we use the BCJR decoder [6] to carry out bit-wise *maximum a posteriori* differential decoding. The BCJR decoder makes a decision on the transmitted symbol (equivalent to a state) based on the maximization

$$\hat{S}[t] = \arg \max_{s \in \{S_1, \dots, S_V\}} P(S[t] = s | z_1^{\tilde{n}}).$$

At each time instant t , the most probable state S_t is computed given the complete received sequence $z_1^{\tilde{n}} = (z[1], z[2], \dots, z[\tilde{n}])$. We will not give a complete derivation of the BCJR algorithm and refer the interested reader to the literature, e.g., [6], [18]. We merely summarize the equations in the Appendix.

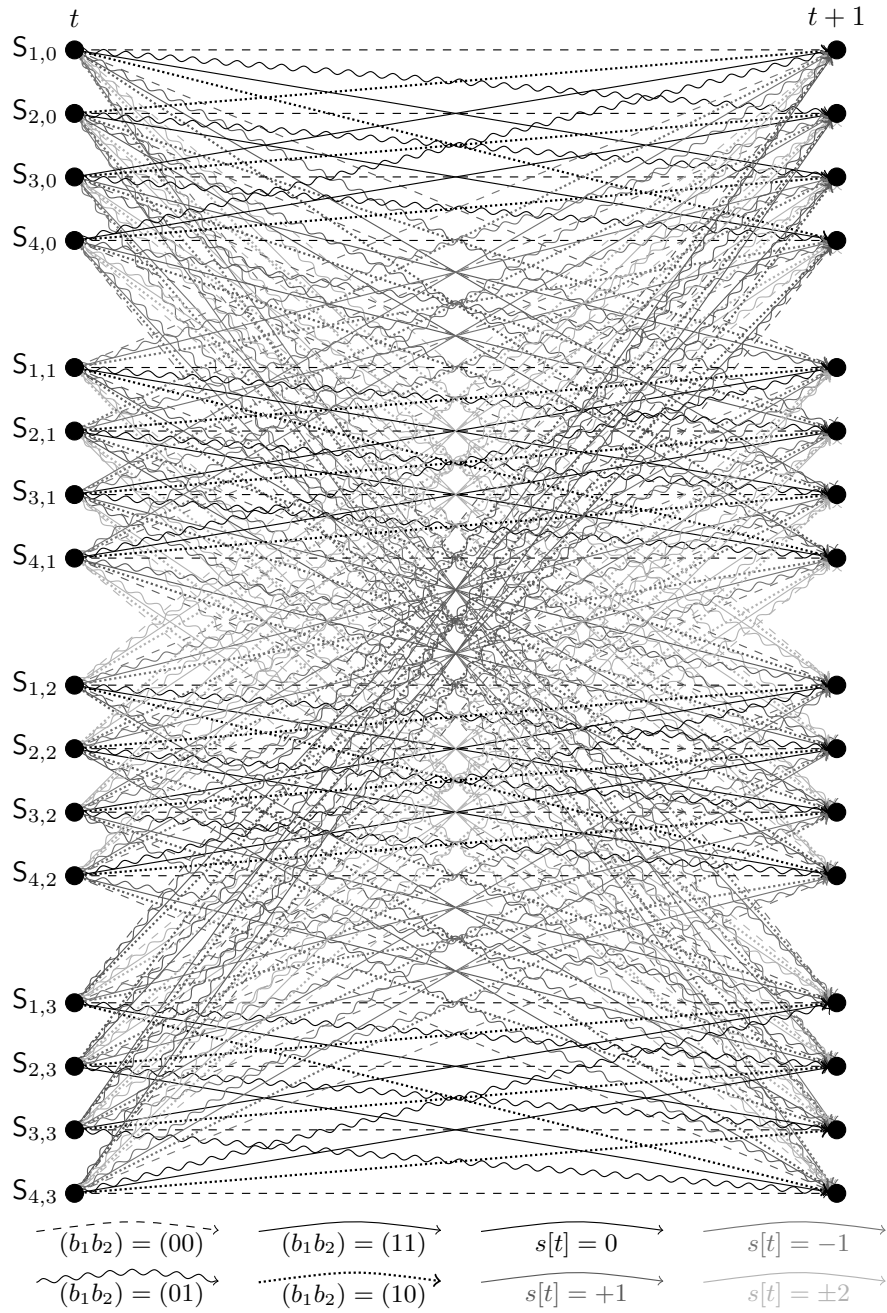


Figure 9: Trellis diagram for *Gray* differential encoding of a constellation with $V = 4$ taking into account the possible phase slips and tracking the phase slip state (indicated by four distinct line types and gray scales)

Table 3: Differential encoding map f_{diff} for the Gray differential code taking into account the phase slip variable $s[t]$

$s[t]$	$(b_{t,1}, b_{t,2})$	$d_{t-1}^{[\text{mem}]} = S_1$	$d_{t-1}^{[\text{mem}]} = S_2$	$d_{t-1}^{[\text{mem}]} = S_3$	$d_{t-1}^{[\text{mem}]} = S_4$
0	(0, 0)	S ₁	S ₂	S ₃	S ₄
0	(0, 1)	S ₂	S ₃	S ₄	S ₁
0	(1, 1)	S ₃	S ₄	S ₁	S ₂
0	(1, 0)	S ₄	S ₁	S ₂	S ₃
1	(0, 0)	S ₂	S ₃	S ₄	S ₁
1	(0, 1)	S ₃	S ₄	S ₁	S ₂
1	(1, 1)	S ₄	S ₁	S ₂	S ₃
1	(1, 0)	S ₁	S ₂	S ₃	S ₄
2	(0, 0)	S ₃	S ₄	S ₁	S ₂
2	(0, 1)	S ₄	S ₁	S ₂	S ₃
2	(1, 1)	S ₁	S ₂	S ₃	S ₄
2	(1, 0)	S ₂	S ₃	S ₄	S ₁
3	(0, 0)	S ₄	S ₁	S ₂	S ₃
3	(0, 1)	S ₁	S ₂	S ₃	S ₄
3	(1, 1)	S ₂	S ₃	S ₄	S ₁
3	(1, 0)	S ₃	S ₄	S ₅	S ₂

We use the technique of *EXtrinsic Information Transfer* (EXIT) charts [19] to characterize the behavior of the differential decoder based on the BCJR algorithm. EXIT charts plot the extrinsic output mutual information as a function of the input mutual information and are a tool to characterize single components in iterative decoders. Bit interleavers statistically decouple the respective encoding/decoding components such that a single parameter is sufficient to track their input/output relations. This parameter may be the signal-to-noise ratio at the output of a processing block, or, as is the case for EXIT charts, the mutual information between transmitted bits and the received and processed soft bit *log-likelihood ratio* (LLR) values. For some channels and some codes, the individual *transfer characteristics* (or EXIT curves) can be obtained analytically, while for most cases, one has to resort to Monte Carlo simulation for computing the mutual information. EXIT curves can be defined not only for channel encoders/decoders such as convolutional codes or parity-check codes, but also for components of many serially or parallel concatenated detection and decoding schemes: For example, EXIT curves have been used for describing channel interfaces such as mappers/demappers (detectors) for spectrally efficient modulation, or equalizers of multipath channels; even the decoder of an LPDC code can be viewed as a serial concatenation, with a variable node decoder and a check node decoder that, both, can be described by EXIT curves, respectively.

The main advantage of the EXIT chart technique is that the individual component processing blocks can be studied and characterized separately using EXIT curves, and that the interaction of two (or more) such processing blocks can be graphically predicted

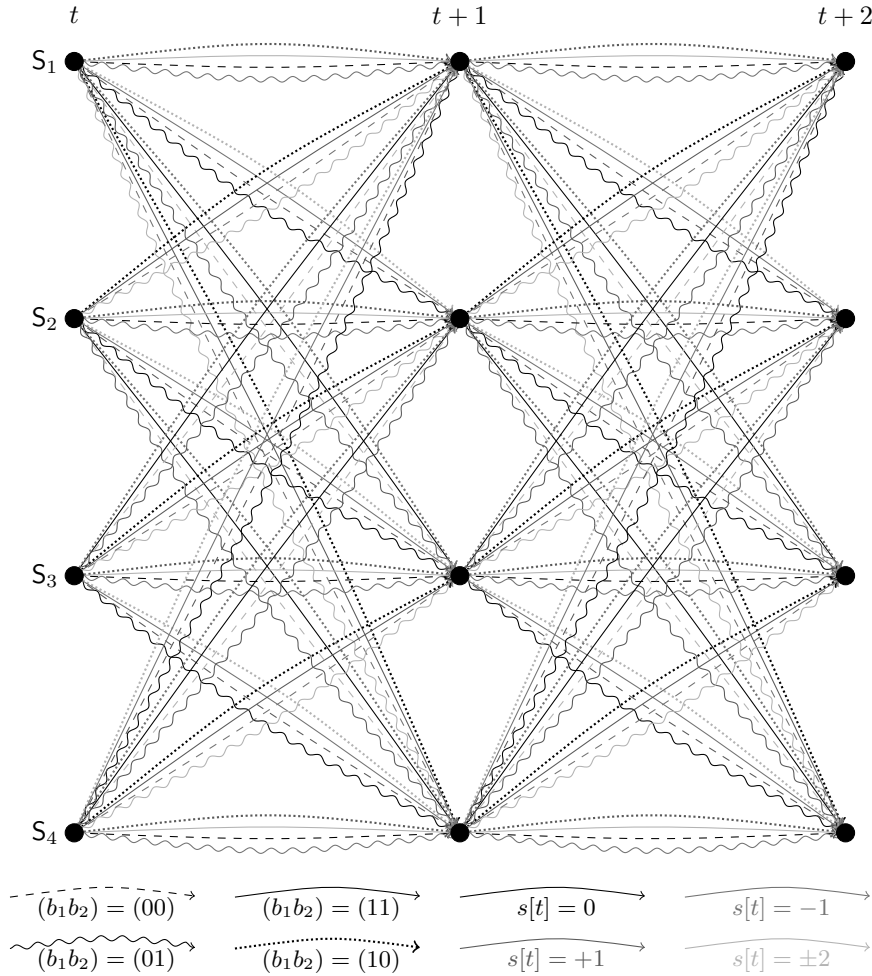


Figure 10: Trellis diagram for *Gray* differential encoding of a constellation with $V = 4$ taking into account the possible phase slip (indicated by four distinct line types and gray scales)

in the EXIT chart without performing a complex simulation of the actual fully-fledged concatenated coding scheme itself. As it turns out, the EXIT curves must not intersect to allow convergence to low bit error rates, and thus, code design reduces to finding good pairs of EXIT curves that match well, or, more constructively as in the case of LDPC codes, to apply curve-fitting algorithms to determine variable and check node degree profiles that match well. A decoding trajectory visualizes the iterative exchange of information between the processing blocks, and shows the progress of the decoding.

While the EXIT chart is exact on the *binary erasure channel* (BEC) for sufficiently long/infinite sequence lengths, the reduction to single parameter tracking of the involved distributions is just an approximation for other channels. It has been observed, however,

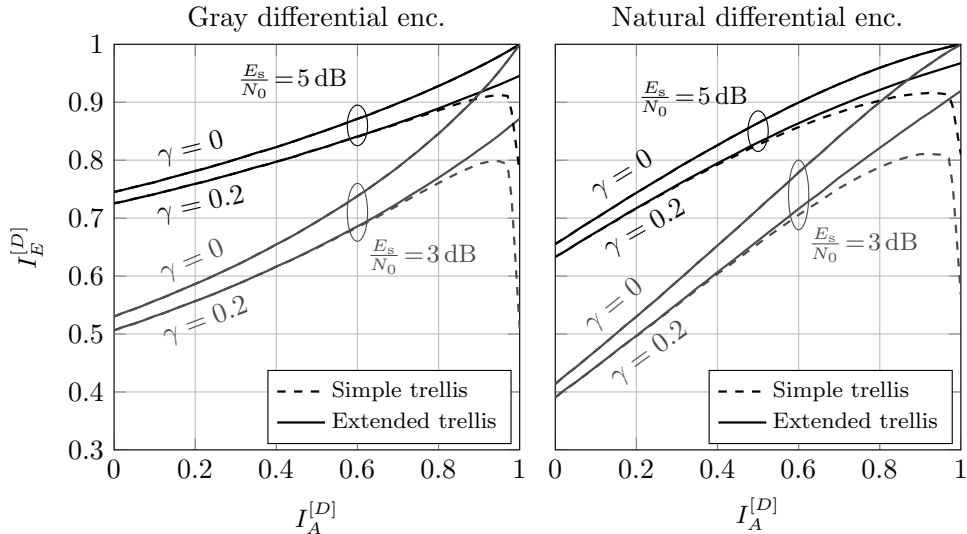


Figure 11: EXIT characteristics of differential detectors using the model-matched decoder with the trellis diagram of Fig. 10 (solid lines, —) and using the conventional unmatched decoder based on the trellis diagram of Fig. 8 (or Fig. 7, respectively) (dashed lines, - - -)

that the predicted and actually simulated decoding trajectories match quite well, proving the usefulness of the method, with many successful code designs performed in practice up to date.

Figure 11 shows the EXIT characteristics of the differential decoder for a QPSK constellation and both differential encoding maps. We can clearly see that the characteristic of the detector employing the non-matched trellis diagram has a non-increasing shape, which is an indicator of a *mismatched model* used within the decoder: the decoder trellis does not leave the possibility open for phase slips to occur, but *forces* the result to a simply differentially encoded target sequence, which, however, is not the case after the phase slip channel. This non-increasing shape is the reason for the error floor that has been observed in [16]. The decreasing EXIT characteristic means that during iterative decoding, the overall system performance actually decreases, which can lead to a severe error floor. In [20], the authors proposed to employ *hybrid turbo differential decoding* (HTDD): by a careful execution of the differential decoder only in those iterations where the extrinsic information is low enough, the operating point in the EXIT chart is in the range of an increasing characteristic. This approach allows the authors of [20] to mitigate the detrimental effect of phase slips on iterative differential decoding and to realize codes with relatively low error floors which can be combated using a high-rate outer code.

If we employ the trellis diagram of Fig. 10 incorporating the phase slip model instead of the non-matched trellis diagram, we can see that the EXIT characteristics are monotonically increasing, which is a prerequisite for successful decoding with low error floors. In the next section, we use the EXIT characteristics to compute the information theoretic achievable rates of the differentially encoded system. Further note that for $\gamma > 0$ (see Sec. 2.2), the

value of $I_E^{[D]} < 1$, even for $I_A^{[D]} = 1$, which may entail an error floor unless the channel code is properly designed.

2.5 Achievable Rates of the Differentially Coded Phase Slip Channel

According to Shannon's information theory [21, 22], the *capacity* of a communication channel is the maximum amount of information (usually expressed in terms of *bits per channel use*) that can be reliably conveyed over the channel. In information theory, the capacity is usually maximized over the input distribution of the channel. In this chapter, we are only interested in the maximum achievable information rate for uniform channel inputs y , as we do not wish to impose any constraints on the data sequence. One possibility to achieve a non-uniform channel input is the use of *constellation shaping* [23, 24], which is however beyond the scope of this chapter. The comparison between the achievable rate of the channel affected by phase slips and the achievable rate of the original AWGN channel shows how much the performance may be sacrificed by the presence of phase slips. In order to compute the achievable rates of the differentially encoded channel affected by phase slips, we employ the EXIT chart technique.

By utilizing a slightly modified way of computing EXIT curves of the BCJR decoder, we can also compute the achievable rates of the coded modulation schemes [25]. For this, we make use of the chain-rule of mutual information [26, 27] and compute the mutual information of the equivalent bit channel experienced by the channel decoder *after* differential detection. This can be done by (numerically, simulation-based) computing the EXIT curve $\tilde{I}_E^{[D]}$ of the differential detector using *a priori* knowledge that is modeled as coming from a BEC, and integrating over such curves. Specifically, EXIT curves like those depicted in Fig. 11 are determined for many different E_s/N_0 -values (and several different phase slip probabilities factors γ) but now with *a priori* knowledge based on a BEC model: By integration, we determine the area $q \int_0^1 \tilde{I}_E^{[D]}(I_A) dI_A$ under these curves [26, 27, 25] and obtain the respective mutual information limits that are plotted into Figs 12 and 13 at the corresponding E_s/N_0 -values and phase slip probabilities factors γ , respectively. Note that this mutual information is available to the channel decoder provided that *perfect* iterative decoding over inner differential detector and outer LDPC decoder is performed. Thus, we still need to design an appropriate LDPC code and iterative decoding scheme to actually approach these promised rates as closely as possible. Indeed, the subsequent sections explain how to construct such codes and coding schemes in more detail. The achievable rate of the non-iterative system with separate differential decoding and channel decoding is obtained from $q\tilde{I}_E^{[D]}(0) = qI_E^{[D]}(0)$.

Figures 12 and 13 show the numerically computed achievable rates for the QPSK constellation *without* differential coding on an AWGN channel that is *not affected* by phase slips (dotted lines, marker “o”) and additionally the achievable rates for differentially encoded QPSK for a channel affected by phase slips (solid lines) with $P_{\text{slip}} = \min\left(1, \frac{\gamma}{2} \operatorname{erfc}\left(\sqrt{\frac{E_s}{2N_0}}\right)\right)$. In Fig. 12 we set $\gamma = 0$ and we observe that the achievable rate of the differential QPSK transmission equals the achievable rate of a conventional coherent QPSK transmission, *in-*

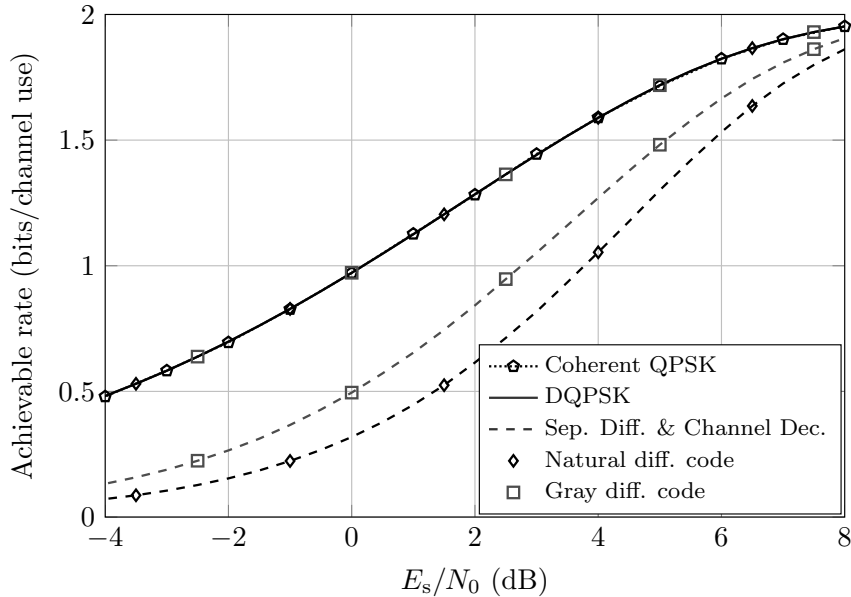


Figure 12: Achievable rates of the DQPSK channel (solid lines, —) and of conventional separate differential & channel decoding (dashed lines, - -) for an AWGN channel without phase slips ($\gamma = 0$)

dependent of the differential encoding map. Additionally, we plot the achievable rates for a simplified system that carries out differential decoding (leading to the well-known effect of error doubling) followed by error correction decoding (dashed lines). We see that at a spectral efficiency of 1.6 (corresponding to system with $\Omega = 25\%$ overhead for coding), the simplified system leads to an unavoidable loss in E_s/N_0 of 1.5 dB (Gray differential encoding map) or 2.5 dB (natural differential encoding map) respectively. This performance difference becomes even more severe if low spectral efficiencies (i.e., high coding overheads) are targeted.

If phase slips occur on the channel ($\gamma > 0$), we can observe in Fig. 13 that for high spectral efficiencies (above 1.5 bits/channel use), the loss in information rate due to the phase slips is not severe, unless γ becomes large. For example, for $\gamma = 0.2$, the capacity loss at a spectral efficiency of 1.5 bit/channel use is only approximately 0.7 dB. The transmission at very low spectral efficiencies, requiring codes with very large overheads, is however seriously affected by the phase slip channel.

3 LDPC Coded Differential Modulation

In the previous section, we have compared the achievable rates of various systems for an AWGN channel ($\gamma = 0$) and we have found that differential coding can be used without entailing a decrease of the communication system's achievable rate. This means that at

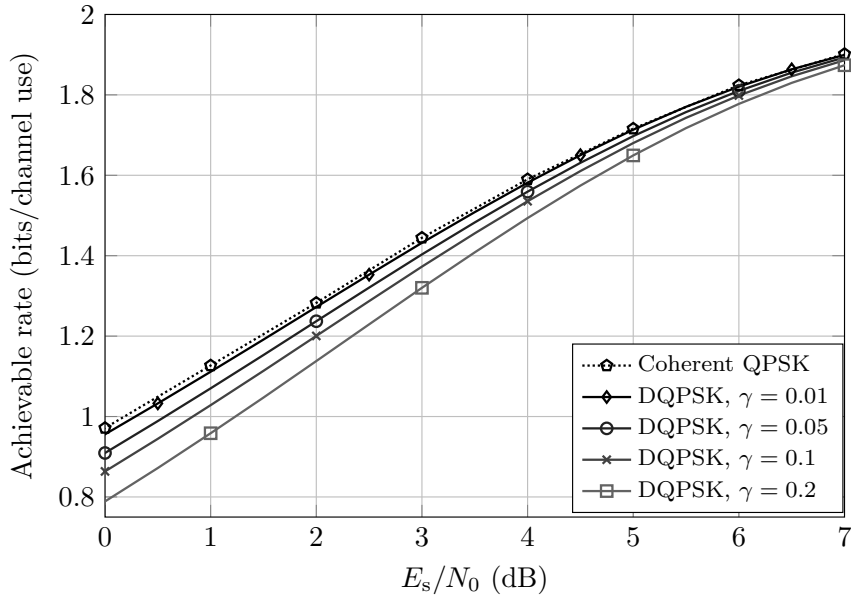


Figure 13: Capacity of the differential DQPSK system for transmission over an AWGN channel affected by phase slips with probability of occurrence depending on pre-FEC bit error rate, given by (3)

least from an information theoretic perspective, we can employ differential coding to combat phase slips without introducing any decoding penalty. Information theory however does not tell us what constructive method we may use to achieve this capacity.

One particularly promising way to approach the capacity with differential coding is the use of coded differential modulation with iterative decoding, as proposed first in [5] with convolutional codes and in [28] with LDPC codes. This scheme extends the *bit-interleaved coded modulation* (BICM) [29] method to account for differential encoding and employs iterative decoding and detection [30, 31] to improve the overall system performance. The adaptation of this scheme to optical communications has been considered in [32] for the channel not affected by phase slips and in [17, 13, 16, 20] for the channel affected by phase slips. Note that other schemes have been proposed that do not rely on iterative differential decoding, including the slip resilient code presented in [33, 34] and block differential modulation [35].

Figure 14 shows the general transmitter (top) and iterative receiver (bottom) of the coded differential modulation system with iterative decoding and detection. In this general block diagram, a block FEC encoder takes as input a binary length- k vector of inputs bits $\mathbf{u} = (u_1, u_2, \dots, u_k)$, where $u_i \in \mathbb{F}_2 = \{0, 1\}$ and generates a binary length- n vector of code bits $\mathbf{x} = (x_1, x_2, \dots, x_n)$. Almost all of the popular channel codes that are used in optical communications are such block codes. The amount $n - k$ of redundant bits that are added by the FEC encoder is commonly expressed in terms of the code rate r which is defined as

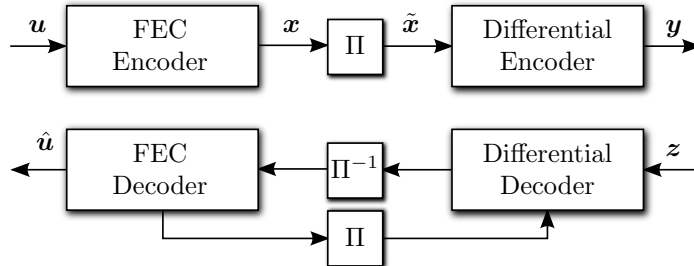


Figure 14: Block diagram of LDPC coded differential modulation transmitter (top) with iterative detector (bottom)

the ratio of the information block length k and the code dimension n , i.e.,

$$r := \frac{k}{n}.$$

In optical communications, often the overhead is used to quantify the amount of redundant information. The overhead Ω of the code and its rate are interrelated by

$$\Omega := \frac{n}{k} - 1 = \frac{n - k}{k} = \frac{1}{r} - 1 = \frac{1 - r}{r}.$$

The block \mathbf{x} of code bits is interleaved by a permutation Π to yield a permuted version $\tilde{\mathbf{x}}$. Ideally, a random permutation is employed, but sometimes, a structure in the permutation is necessary to facilitate implementation (parallelization) or to improve the error correction capabilities of the code. Note that the permutation Π is sometimes implicitly included in the FEC encoder and does not need to be explicitly implemented. The interleaved block $\tilde{\mathbf{x}}$ is differentially encoded (as discussed in Sec. 2.3) yielding a block of $\tilde{n} = \lceil \frac{n}{q} \rceil$ modulation symbols (where $\lceil \tau \rceil$ denotes the smallest integer larger or equal than τ).

At the receiver, the differential decoder and the FEC decoder iteratively decode the signal, where the output of the FEC decoder is used to yield an improved differential decoding result in a subsequent iteration by sharing so-called *extrinsic information* between the decoder components. For a thorough description and introduction to the concept of iterative detection and decoding we refer the interested reader to [36, 18]. In the remainder of this section, we assume that the employed FEC scheme is a low-density parity-check (LDPC) [37, 18] code. We will first give an introduction to LDPC codes and then show how irregular LDPC codes can be designed to be well-adapted to differential coding. We do not show explicitly how decoding is performed, as we intend to take on a more code design-oriented perspective. We will only give equations for performing differential decoding and LDPC decoding in the Appendix.

We restrict ourselves in the remainder of this chapter to the case where $V = Q = 2^q$, i.e., every state \mathbf{S}_i is assigned to the modulation symbol M_i . We will however give hints on how to deal with the case $V < Q$ in Sec. 3.3.

3.1 Low-Density Parity-Check (LDPC) Codes

Low-density parity-check (LDPC) codes were developed in the 1960s by Gallager in his landmark Ph.D. thesis [37]. These codes were not further investigated for a long time due to the perceived complexity of long codes. With the discovery of turbo codes in 1993 [38] and the sudden interest in iteratively decodable codes, LDPC codes were rediscovered soon afterwards [39, 40]. In the years that followed, numerous publications from various researchers paved the way for a thorough understanding of this class of codes leading to numerous applications in various communication standards, such as, e.g., WLAN (IEEE 802.11) [41], DVB-S2 [42], and 10G Ethernet (IEEE 802.3) [43]. LDPC codes for soft-decision decoding in optical communications were studied in [44]. Modern high-performance FEC systems are sometimes constructed using a soft-decision LDPC inner code which reduces the BER to a level of 10^{-3} to 10^{-5} and a hard-decision outer code which pushes the system BER to levels below 10^{-12} [44]. An outer cleanup code is used as most LDPC codes exhibit a phenomenon called *error floor*: above a certain *signal-to-noise ratio* (SNR), the BER does not drop rapidly anymore but follows a curve with a small slope. This effect is mainly due to the presence of *trapping sets* or *absorbing sets* [45, 46]. The implementation of a coding system with an outer cleanup code requires a thorough understanding of the LDPC code and a properly designed interleaver between the LDPC and outer code for avoiding that the errors at the output of the LDPC decoder—which typically occur in clusters—cause uncorrectable blocks after outer decoding. With increasing computing resources, it is now also feasible to evaluate very low target BERs of LDPC codes and optimize the codes to have very low error floors below the system’s target BER [47]. A plethora of LDPC code design methodologies exist, each with its own advantages and disadvantages. The goal of an LDPC code designer is to find a code that yields high coding gains and which possesses some structure facilitating the implementation of the encoder and decoder. We point the interested reader to numerous articles published on this topic, e.g., [48, 49, 50] and references therein. An introduction to LDPC codes in the context of optical communications is given in [51]. An overview of coding schemes for optical communications is also provided in [12] and the references therein. For a thorough reference to LDPC codes together with an overview of decoding algorithms and construction methods, we refer the interested reader to [18].

An LDPC code is defined by a sparse binary parity check matrix \mathbf{H} of dimension $m \times n$, where n is the code word length (in bits) of the code and m denotes the number of parity check equations defining the code. Usually⁴, the number of information bits equals $n - m$. The overhead of the code is defined as $\Omega = \frac{m}{n-m}$. A related measure is the *rate* of the code, which is defined as $r = \frac{n-m}{n}$. Sparse means that the number of “1”s in \mathbf{H} is small compared to the number of zero entries. Practical codes usually have a fraction of “1”s that is below 1% by several orders of magnitude. We start by introducing some notation and terminology related to LDPC codes. Each column of the parity check matrix \mathbf{H} corresponds to one bit of

⁴provided that the parity-check matrix has full row rank, i.e., $\text{rank } \mathbf{H} = m$. If the parity-check matrix \mathbf{H} is rank-deficient, the number of information bits $k \geq n - m$

the FEC frame. The n single bits of the code are also often denoted as *variables*. Similarly, each row of \mathbf{H} corresponds to a parity check equation and ideally defines a single parity bit (if \mathbf{H} has full rank).

3.1.1 Regular and Irregular LDPC Codes

LDPC codes are often classified into two categories: regular and irregular LDPC codes. In this chapter, we consider the latter, which also constitutes the more general, broader class of codes. The parity check matrix of regular codes has the property that the number of “1”s in each column is constant and amounts to v_{reg} . (called *variable degree*) and that the number of “1”s in each row is constant and amounts to c_{reg} . (called *check degree*). Clearly, $n \cdot v_{\text{reg}} = m \cdot c_{\text{reg}}$. has to hold and we furthermore have $r = 1 - \frac{v_{\text{reg}}}{c_{\text{reg}}}$. Irregular LDPC codes [52] have the property that the number of “1”s in the different columns of \mathbf{H} is not constant. In this chapter, we mainly consider *column-irregular* codes, which means that only the number of “1”s in the columns is not constant but the number of “1”s in each row remains constant. The irregularity of the parity-check matrix is often characterized by the degree profile of the parity check matrix \mathbf{H} [50].

We denote the number of columns of the parity-check matrix \mathbf{H} with i ones by Λ_i . We say that these columns have *degree* i . Normalizing this value to the number of total bits n per codewords yields

$$L_i = \frac{\Lambda_i}{n},$$

which is the *fraction* of columns with degree i , i.e., with i ones (e.g., if $L_3 = \frac{1}{2}$, half the columns of \mathbf{H} have three “1”s).

Similarly, we can define the *check degree profile* by defining that P_j denotes the number of rows of \mathbf{H} with exactly j “1”s. The normalized check profile is given by R_j , the *fraction* of rows with j “1”s. We have the $R_j = \frac{P_j}{m}$. In most of the codes we consider, however, *all* rows of \mathbf{H} have the same number of c_{reg} “1”s. In that case, we have $R_{c_{\text{reg}}} = 1$ and $R_1 = R_2 = \dots = R_{c_{\text{reg}}-1} = R_{c_{\text{reg}}+1} = \dots = R_{\infty} = 0$. Example 3.1 illustrates the degree distribution of such an irregular LDPC code.

Example 3.1 Consider the following LDPC code of size $n = 32$ with parity-check matrix of size $\dim \mathbf{H} = m \times n = 8 \times 32$, i.e., of rate $r = \frac{32-8}{32} = 0.75$, corresponding to an overhead of 33.3%. Note that the zeros in \mathbf{H} are not shown for clarity.

$$\mathbf{H} = \left(\begin{array}{cccc|cccc|cccc|cccc} 1 & 1 & & & 1 & 1 & 1 & & 1 & 1 & 1 & 1 & 1 & 1 & 1 & 1 & 1 & 1 \\ 1 & 1 & & & 1 & 1 & 1 & 1 & & & 1 & 1 & 1 & 1 & 1 & 1 & 1 & 1 \\ & 1 & 1 & & 1 & 1 & 1 & 1 & & & 1 & & 1 & 1 & 1 & 1 & 1 & 1 \\ & & 1 & 1 & 1 & & 1 & 1 & 1 & 1 & & & 1 & 1 & 1 & 1 & 1 & 1 \\ & & & 1 & 1 & & 1 & 1 & 1 & 1 & & & 1 & 1 & 1 & 1 & 1 & 1 \\ & & & & 1 & 1 & 1 & 1 & & & 1 & 1 & 1 & 1 & 1 & 1 & 1 & 1 \\ & & & & & 1 & 1 & 1 & & & 1 & 1 & 1 & 1 & 1 & 1 & 1 & 1 \\ & & & & & & 1 & 1 & 1 & & & & 1 & 1 & 1 & 1 & 1 & 1 \end{array} \right)$$

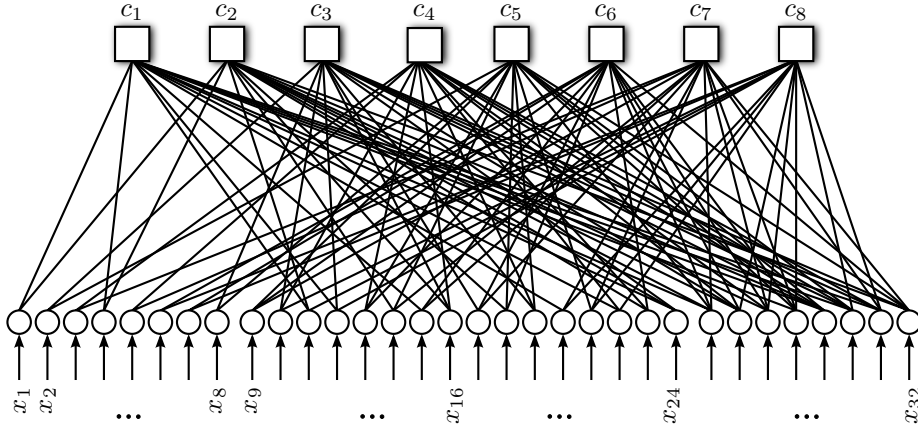


Figure 15: Graph of the code defined by the parity check matrix given in Example 3.1

The first 8 columns of \mathbf{H} have two “1”s per column, i.e., $\Lambda_2 = 8$. Furthermore, the middle 16 columns each contain three “1”s, i.e., $\Lambda_3 = 16$. Finally, the last 8 columns contain five “1”s, i.e., $\Lambda_5 = 8$. Normalizing leads to

$$L_2 = \frac{\Lambda_2}{n} = \frac{1}{4}, \quad L_3 = \frac{\Lambda_3}{n} = \frac{1}{2}, \quad L_5 = \frac{\Lambda_5}{n} = \frac{1}{4}.$$

Note that $L_1 = L_4 = L_6 = L_7 = \dots = 0$. The number of “1”s in each row of \mathbf{H} is constant and amounts to $c_{\text{reg.}} = 13$.

3.1.2 Graph Representation of LDPC Codes

LDPC codes are often represented by a so-called *Tanner* graph [50]. This graph is an undirected bipartite graph in which the nodes can be partitioned into two disjoint sets and each edge connects a node from the first set to a node from the second set. The Tanner graph allows for an easy description of the decoding algorithm of LDPC codes, which we will not detail here. We will give a summary of the iterative decoding algorithm in the Appendix. Figure 15 shows the graph representation of the toy code given in Example 3.1. The circular nodes on the bottom of the graph represent the *variable nodes*, which correspond to the bits in the codeword. As each codeword contains n bits, there are n variable nodes x_1, x_2, \dots, x_n . The variable node x_i has one connection to the transmission channel (arrow from the bottom) and j additional connections towards the top where j equals the number of “1”s in the i th column of \mathbf{H} . For instance, the first Λ_2 variables $x_1, \dots, x_{\Lambda_2}$ (where $\Lambda_2 = 8$) of the code have 2 connections towards the graph part of the code and an additional connection from the transmission channel. As in Example 3.1, the variable nodes can be divided into three groups, corresponding to the degree of these variables.

The rectangular nodes on the top of the graph are the so called *check nodes*. Each check node c_i corresponds to one of the m rows of the parity-check matrix \mathbf{H} of the code and

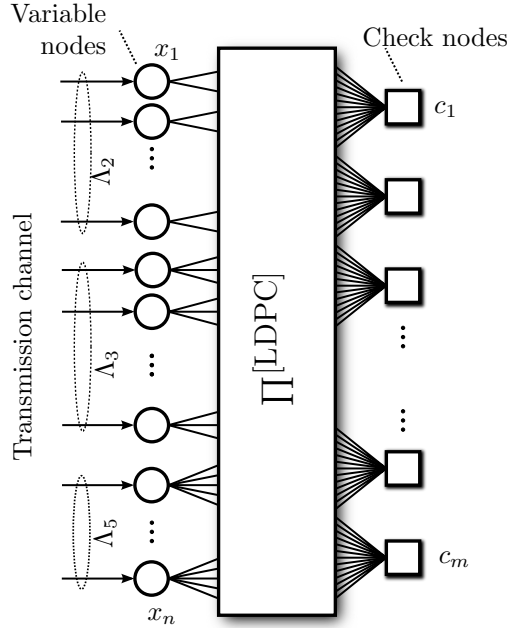


Figure 16: Simplified graph representation of an irregular LDPC code with $v \in \{2, 3, 8\}$ and $c_{\text{reg.}} = 8$

defines a code *constraint*. The number of connections of the check nodes with the graph corresponds to the number of “1”s in the respective row of \mathbf{H} . In the above example, every row has $c_{\text{reg.}} = 13$ “1”s, so that each of the check nodes has exactly $c_{\text{reg.}} = 13$ connected edges. If \mathbf{H} has a non-zero entry at row i and column j , i.e. $H_{i,j} = 1$, then an edge connects variable node x_j to check node c_i .

As drawing the graph of the code in this way quickly becomes cumbersome and confusing due to the large number of edges, we resort to a simplified (and rotated) representation shown in Fig. 16. In this figure, we do not draw all the edges, but only the beginning and end of each edge and assume that the permutation of the edges is managed by an interleaver $\Pi^{\text{[LDPC]}}$. The interleaver $\Pi^{\text{[LDPC]}}$ thus ensures that the connections between the different nodes corresponds to the one given by the parity-check matrix \mathbf{H} .

3.1.3 Design of Irregular LDPC Codes

The design of irregular LDPC codes consists of finding good degree distributions, i.e. good values Λ_i and P_i (or $c_{\text{reg.}}$) such that the rate of the code has the desired value (given by the system designer) and such that the NCG achievable by this code is maximized, i.e., the code is able to successfully recover the bit stream at the lowest possible E_s/N_0 value. A comprehensive body of literature on the design of irregular codes exists (see [18] and references therein) and we only introduce the basics to describe the optimization of codes

tailored to slip-tolerant differential decoding in Sec. 3.2.

The optimization of irregular LDPC codes requires the use of *edge-perspective* degree distributions [50].

Definition 3 (Edge-perspective degree distribution) *In the Tanner graph representation of the code, we denote by λ_i the fraction of edges that are connected to variable nodes of degree i . We have*

$$\lambda_i = \frac{i \cdot L_i}{\sum_{j=1}^{\infty} j \cdot L_j}. \quad (4)$$

Similarly, ρ_i denotes the fraction of edges that are connected to check nodes of degree i . Again, we have

$$\rho_i = \frac{i \cdot R_i}{\sum_{j=1}^{\infty} j \cdot R_j}.$$

Using the technique of EXIT charts [19, 27, 53], good values of λ_i and potentially ρ_i may be found that can then be used to design a parity-check matrix \mathbf{H} fulfilling these degree distributions. We constrain the maximum possible variable node degree to be v_{\max} and the maximum possible check node degree to be c_{\max} .

The inverse relationship between λ_i and L_i , or between ρ_i and R_i , respectively, reads

$$L_i = \frac{\frac{\lambda_i}{i}}{\sum_{j=1}^{v_{\max}} \frac{\lambda_j}{j}} \quad \text{and} \quad R_i = \frac{\frac{\rho_i}{i}}{\sum_{j=1}^{c_{\max}} \frac{\rho_j}{j}}. \quad (5)$$

The (iterative) LDPC decoding process may be understood as a process where two decoders pass information between each other. The first decoder is the *variable node decoder* (VND) which processes each of the n variable nodes of the code. The second decoder is the *check node decoder* (CND), which processes each of the m check nodes. Each of these decoders has a certain *information transfer* (EXIT) characteristic. Before describing the transfer characteristics, we introduce the J -function that interrelates mean μ (and variance, which amounts 2μ in the case of symmetric messages, for details, see [19] and [50]) and mutual information for the Gaussian random variable describing the messages that are exchanged in the iterative decoder, with

$$J(\mu) = 1 - \int_{-\infty}^{\infty} \frac{e^{-(\tau-\mu)^2/(4\mu)}}{\sqrt{4\pi\mu}} \log_2(1 + e^{-\tau}) d\tau$$

which can be conveniently approximated [54] by

$$I = J(\mu) \approx \left(1 - 2^{-H_1(2\mu)^{H_2}}\right)^{H_3}$$

$$\mu = J^{-1}(I) \approx \frac{1}{2} \left(-\frac{1}{H_1} \log_2 \left(1 - I^{\frac{1}{H_3}}\right) \right)^{\frac{1}{H_2}}$$

with $H_1 = 0.3073$, $H_2 = 0.8935$, and $H_3 = 1.1064$.

In the case of LDPC codes and transmission over an AWGN channel, the information transfer characteristics are obtained as [55]

$$I_E^{[V]} = f_V \left(I_A^{[V]}, \frac{E_s}{N_0} \right) := \sum_{i=1}^{v_{\max}} \lambda_i J \left(4 \frac{E_s}{N_0} + (i-1) J^{-1}(I_A^{[V]}) \right) \quad (6)$$

$$I_E^{[C]} = f_C(I_A^{[C]}) := \sum_{i=1}^{c_{\max}} \frac{\rho_i}{\log(2)} \sum_{j=1}^{\infty} \frac{\left(\Phi_j \left(J^{-1}(I_A^{[C]}) \right) \right)^{i-1}}{2j(2j-1)} \quad (7)$$

where

$$\Phi_i(\mu) = \int_{-1}^1 \frac{2\tau^{2i}}{(1-\tau^2)\sqrt{4\pi\mu}} \exp \left(-\frac{\left(\mu - \log \frac{1+\tau}{1-\tau} \right)^2}{4\mu} \right) d\tau.$$

Equation (6) describes the characteristic of the VND while (7) describes the characteristic of the CND. For codes with regular check node degree, (7) can be simplified to

$$I_E^{[C]} = f_C(I_A^{[C]}) := \frac{1}{\log(2)} \sum_{j=1}^{\infty} \frac{\left(\Phi_j \left(J^{-1}(I_A^{[C]}) \right) \right)^{c_{\text{reg.}}-1}}{2j(2j-1)}$$

As $I_A^{[V]} = I_E^{[C]}$ holds in the context of iterative decoding, a condition for successful decoding is that

$$f_V \left(I, \frac{E_s}{N_0} \right) > f_C^{-1}(I), \quad \forall I \in [0; 1] \quad (8)$$

where the inverse function $f_C^{-1}(I)$ of the strictly monotonically increasing function f_C given in (7) can be found using numerical methods. The task of the code designer is to find a degree distribution minimizing E_s/N_0 such that (8) is fulfilled. Usually, the condition (8) is evaluated at discrete values of I only, simplifying the implementation.

Some more conditions usually apply to the degree distributions. One of these is the so-called *stability condition* [50], which, in the case of an AWGN channel ensures that

$$\lambda_2 \leq \frac{\exp \left(\frac{E_s}{N_0} \right)}{\sum_{i=1}^{c_{\max}} \rho_i (i-1)}.$$

3.2 Code Design for Iterative Differential Decoding

As described in Sec. 2.5, the differential decoder based on the BCJR algorithm can be characterized by an EXIT characteristic $I_E^{[D]} = f_D(I_A^{[D]}, E_s/N_0)$. Before optimizing the LDPC code towards the interworking with the differential decoding, we first have to define the *decoder scheduling* as we are concerned with a three-fold iterative decoder loop: decoding iterations are carried out within the LDPC decoder and between LDPC decoder and differential decoder. In this chapter, we restrict ourselves to the following scheduling:

- a) In a first initial step, the differential decoder is executed and generates initial channel-related information.
- b) Using this initial channel-related information, a *single* LDPC iteration is carried out, i.e., a single execution of the check node and variable node computing processors.
- c) Using the accumulated variable node information from the LDPC graph, *excluding* the intrinsic channel-related information from the initial differential decoding execution (step a)), the differential decoder is executed again, yielding improved channel-related information.
- d) With the improved information from step c), another *single* LDPC iteration is carried out. If the maximum number of allowed iterations is not yet reached, we continue with step c).
- e) If the maximum number of iterations is reached, the accumulated variable node information is used to get an *a posteriori* estimate of each bit.

In what follows, we now describe in detail how to find good degree distributions for iterative differential decoding. In [56] and [57], conditions for degree distributions were derived and it was analyzed if it is possible to construct codes that work equally well for differential coding and conventional non-differential transmission. In this work, we solely consider the case of differential coding and we aim at showing different possibilities of degree distribution optimization with the goal to show the best possibility for LDPC coded differential modulation with the above mentioned decoder scheduling.

We only consider *column irregular* codes in the remainder of this chapter, i.e., the number of “1”s in each row of the parity-check matrix \mathbf{H} is constant and amounts to c_{reg} . Such a constraint is often imposed as it simplifies the hardware that is needed to implement the check node decoding operation, which is the most difficult operation in the LDPC decoder. The complexity of this operation scales roughly linearly with the check node degree (i.e., the number of “1”s per row) and having a constant degree allows the hardware designer to implement a fixed and optimized check node computation engine. The second constraint that we impose is that we only have three different variable node degrees, namely Λ_2 variable nodes of degree 2, Λ_3 variable nodes of degree 3, and $\Lambda_{v_{\text{max}}}$ variable nodes of degree v_{max} . This is in line with the findings given in [58] that show that the degree distributions are often sparse and that only a few different values are often sufficient. Having only three different variable node degrees simplifies the hardware implementation, especially the design of the required bit widths in a fixed point implementation.

Contrary to many degree distribution approaches proposed in the literature [50, 56, 59] we first fix the rate r of the final code as the rate is usually constrained by the system design parameters (e.g., speed of analog-to-digital and digital-to-analog converters, pulse shape, channel bandwidth, framing overhead, etc.). With fixed rate r , we remove the dependencies [58] of the degree distribution. We further assume that no nodes of degree 1 are present in the code, i.e., $\Lambda_1 = 0$ and thus $\lambda_1 = 0$. As $\sum_i \lambda_i = 1$, we can uniquely

determine λ_2 as

$$\lambda_2 = 1 - \sum_{i=3}^{v_{\max}} \lambda_i. \quad (9)$$

As the rate of the code is given by [50]

$$r = 1 - \frac{\sum_{i=1}^{c_{\max}} \frac{\rho_i}{i}}{\sum_{i=1}^{v_{\max}} \frac{\lambda_i}{i}} \quad (10)$$

we can eliminate another dependency and by combining (10) with (9), we get

$$\lambda_3 = 3 + 6 \sum_{i=4}^{v_{\max}} \lambda_i \left(\frac{1}{i} - \frac{1}{2} \right) - \frac{6}{1-r} \sum_{i=1}^{c_{\max}} \frac{\rho_i}{i}. \quad (11)$$

For check-regular codes with regular check node degree c_{reg} . (i.e., $\rho_{c_{\text{reg}}} = 1$), (11) can be simplified to

$$\lambda_3 = 3 - 6 \left(\frac{1}{c_{\text{reg}}(1-r)} - \sum_{i=4}^{v_{\max}} \lambda_i \left(\frac{1}{i} - \frac{1}{2} \right) \right). \quad (12)$$

This means that λ_2 and λ_3 are uniquely determined by $\lambda_4, \lambda_5, \dots, \lambda_{v_{\max}}$. If we only allow λ_2, λ_3 and $\lambda_{v_{\max}}$ to be nonzero, then λ_2 and λ_3 are uniquely determined by $\lambda_{v_{\max}}$ and we have

$$\lambda_3 = 3 - 6 \left(\frac{1}{c_{\text{reg}}(1-r)} - \lambda_{v_{\max}} \left(\frac{1}{v_{\max}} - \frac{1}{2} \right) \right) \quad (13)$$

$$\lambda_2 = -2 - \lambda_{v_{\max}} + 6 \left(\frac{1}{c_{\text{reg}}(1-r)} - \lambda_{v_{\max}} \left(\frac{1}{v_{\max}} - \frac{1}{2} \right) \right). \quad (14)$$

For determining the degree distribution, the choice of the interleaving scheme between LDPC code and differential encoder/decoder is crucial. In fact, this choice determines how to select the degree distribution and finally has an influence on the overall system performance.

3.2.1 Design of LDPC Codes – Full Interleaving

The first way of interleaving consists in placing a full interleaver $\Pi^{[\text{diff}]}$ of size n between differential code and LDPC code, as depicted in Fig. 17. The interleaver $\Pi^{[\text{diff}]}$ is placed between the differential decoder and the variable nodes of the LDPC code, such that the interleaved output of the differential decoder mimics the transmission channel output. This is the approach that has been followed in [59] and [28].

As the transmission channel is in this case the combination of differential decoder and interleaver, we need to modify the convergence condition (8). Instead of having a function

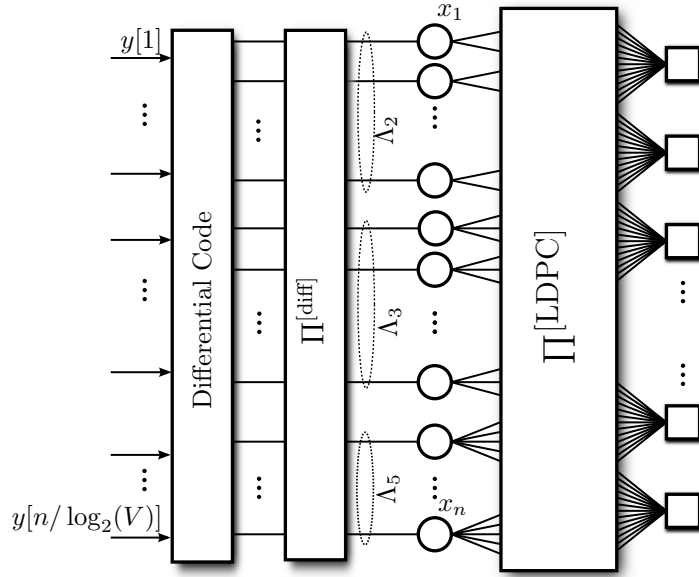


Figure 17: Schematic of the LDPC code with full interleaving between LDPC code and differential decoder

describing the information transfer of the VND, we introduce a function $f_{V,D}$ that describes the information transfer of the combined differential decoder and VND. This combined information transfer function is given by

$$I_E^{[V,D]} = \sum_{i=1}^{v_{\max}} \lambda_i J \left(\mu_c + (i-1)J^{-1}(I_A^{[V,D]}) \right)$$

The value μ_c is the mean of the message that is sent from the differential decoder towards the LDPC code. Using the EXIT characteristic of the differential decoder $f_D(I, E_s/N_0)$, which can be prerecorded and potentially represented by a polynomial [53], we can express μ_c as [53]

$$\mu_c = J^{-1} \left(f_D \left(\sum_{i=1}^{v_{\max}} L_i J \left(i \cdot J^{-1}(I_A^{[V,D]}) \right), \frac{E_s}{N_0} \right) \right)$$

which leads to the overall EXIT characteristic of the combined VND and differential decoder

$$\begin{aligned} f_{V,D} \left(I, \frac{E_s}{N_0} \right) &= \sum_{i=2}^{v_{\max}} \lambda_i J \left(J^{-1} \left(f_D \left(\sum_{j=2}^{v_{\max}} L_j J \left(j \cdot J^{-1}(I_A^{[V,D]}) \right), \frac{E_s}{N_0} \right) \right) + (i-1)J^{-1}(I_A^{[V,D]}) \right) \\ &= \sum_{i=2}^{v_{\max}} \lambda_i J \left(J^{-1} \left(f_D \left(\sum_{j=2}^{v_{\max}} \frac{\lambda_j J \left(j \cdot J^{-1}(I_A^{[V,D]}) \right)}{j \sum_{\kappa=2}^{v_{\max}} \frac{\lambda_{\kappa}}{\kappa}}, \frac{E_s}{N_0} \right) \right) + (i-1)J^{-1}(I_A^{[V,D]}) \right) \end{aligned} \quad (15)$$

where we have used (5) in the second line of the equation. This leads to the condition for successful decoding

$$f_{V,D} \left(I, \frac{E_s}{N_0} \right) > f_C^{-1}(I), \quad \forall I \in [0; 1]. \quad (16)$$

In this case, the stability condition reads [59]

$$\lambda_2 < \frac{1}{c_{\text{reg.}} - 1} \exp \left(\frac{J^{-1} \left(f_D \left(1, \frac{E_s}{N_0} \right) \right)}{4} \right) \quad (17)$$

As the function $f_{V,D}(\cdot, \cdot)$ is not linear in λ_i (and even not necessarily convex), the elegant linear programming based optimization [50] cannot be applied. We have to resort to heuristic optimization methods such as *differential evolution* [58] or *simulated annealing*. If we assume however that the degree distribution only consists of three degrees 2, 3 and v_{max} , then we have seen before that by fixing $\lambda_{v_{\text{max}}}$, the values of λ_2 and λ_3 are immediately given. Thus the problem of finding the optimal degree distribution reduces to a one-dimensional problem. By sweeping $\lambda_{v_{\text{max}}}$ between the extremes of the admissible interval $[0, 1]$, we can find the best possible degree distribution.

We use the following binary search to find the best possible degree distribution. We first assume that the differential decoder EXIT characteristic is available for any E_s/N_0 value between $\frac{E_s}{N_0}|_{\text{min}}$ and $\frac{E_s}{N_0}|_{\text{max}}$. We fix a minimum step size Δ_{min} and use Algorithm 1 which outputs the optimum $c_{\text{reg.}}$, λ_2 , λ_3 and $\lambda_{v_{\text{max}}}$. We have found that using only three different variable node degrees and only a fixed check node degree does not impose a noteworthy limitations and that the performance of the obtained codes is very close to the performance of codes designed with less constraints, provided that v_{max} is chosen large enough.

The full interleaving scheme has several limitations. For instance, the EXIT chart based optimization assumes that the messages exchanged between the different decoder components are Gaussian distributed. This is however not the case when interleaving the outputs of all different variables; in this case, the messages show rather a distribution that can be described by a *Gaussian mixture*, leading to inaccuracies of the model. Even though the messages may be conveniently approximated by Gaussian distributions (if the variances of the different parts of the mixture do not vary much), the codes designed according to this model may not yield the best possible performance.

3.2.2 Design of LDPC Codes – Partial Interleaving

In order to mitigate the limitations of the full interleaving approach of the previous paragraph, we replace the single interleaver $\Pi^{\text{[diff]}}$ by multiple *partial* interleavers, as described in [60] and inspired by the analysis for BICM-ID with convolutional codes in [61]. In the partial interleaving case, we group all Λ_i variable nodes of degree i , assign an interleaver of size Λ_i to these nodes and employ a separate differential decoder/encoder for this group of variable nodes. The graph-based model with partial interleaving is shown in Fig. 18 (where we assume that each Λ_i is a multiple of V).

Algorithm 1: Binary search for finding good LDPC code degree distribution

Input: Maximum variable node degree v_{\max}

Input: Minimum and maximum check node degrees c_{\min} and c_{\max}

Input: Discretization steps D (mutual information) and D_λ

Input: Minimum stepsize Δ_{\min}

Output: Optimum variable node degree distribution $\lambda_{\text{best}} = (\lambda_2, \lambda_3, \lambda_{v_{\max}})$

Output: Optimum check node degree c_{best}

Output: SNR threshold E_{best}

```
1 begin
2    $E \leftarrow \frac{1}{2} \left( \frac{E_s}{N_0} \Big|_{\min} + \frac{E_s}{N_0} \Big|_{\max} \right)$ ,  $E_{\text{best}} \leftarrow \infty$ ,  $\Delta \leftarrow \frac{1}{2} \left( \frac{E_s}{N_0} \Big|_{\max} - \frac{E_s}{N_0} \Big|_{\min} \right)$ 
3   while  $\Delta > \Delta_{\min}$  do
4     Success  $\leftarrow$  false
5     for  $c_{\text{reg.}} = c_{\min} \dots c_{\max}$  do
6       compute  $f_C^{-1} \left( \frac{i}{D}, c_{\text{reg.}} \right)$ ,  $\forall i \in \{0, 1, \dots, D-1\}$ 
7       for  $j \in \{0, 1, \dots, D_\lambda\}$  do
8          $\lambda_{v_{\max}} \leftarrow \frac{j}{D_\lambda}$ 
9         determine  $\lambda_2$  and  $\lambda_3$  via (14) and (13)
10        compute  $f_{V,D} \left( \frac{i}{D}, E \right)$ ,  $\forall i \in \{0, \dots, D-1\}$  using (15)
11        if  $f_{V,D} \left( \frac{i}{D}, E \right) > f_C^{-1} \left( \frac{i}{D} \right)$ ,  $\forall i$  and (17) fulfilled then
12          if  $E < E_{\text{best}}$  then
13             $E_{\text{best}} \leftarrow E$ 
14             $\lambda_{\text{best}} = (\lambda_2, \lambda_3, \lambda_{v_{\max}})$ 
15             $c_{\text{best}} \leftarrow c_{\text{reg.}}$ 
16          end
17          Success  $\leftarrow$  true
18        end
19      end
20    end
21    if Success = True then
22       $E \leftarrow E - \frac{\Delta}{2}$ 
23    else
24       $E \leftarrow E + \frac{\Delta}{2}$ 
25    end
26     $\Delta \leftarrow \frac{\Delta}{2}$ 
27  end
28 end
```

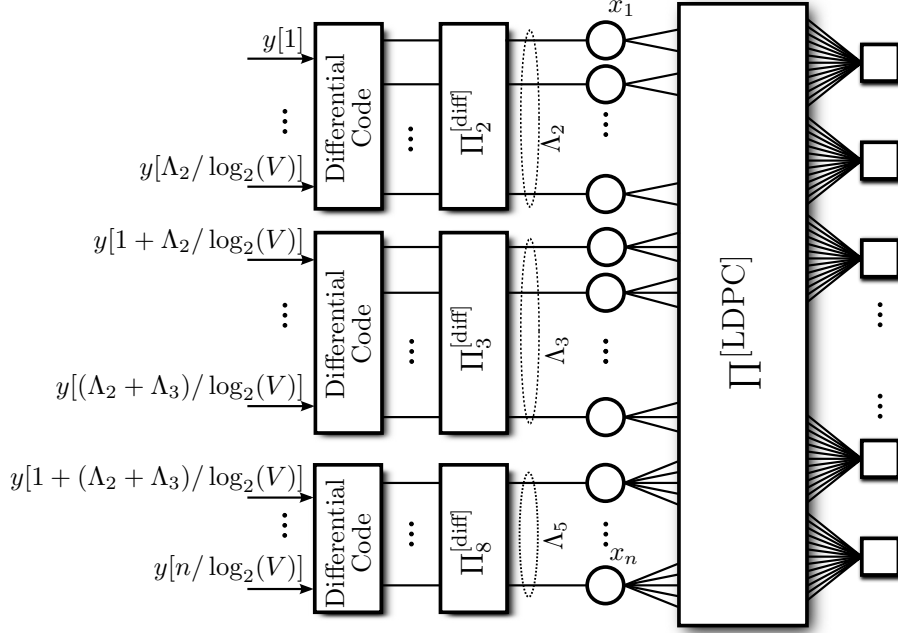


Figure 18: Schematic of the LDPC code with partial interleaving between LDPC code and differential decoder

If partial interleaving is used, the equations for analyzing the convergence and finding good degree distributions have to be modified as well. In this case, every variable node group (of degree i) has to be treated separately and is assigned its own differential decoder output $\mu_{c,i}$ and we can write

$$I_E^{[V,D]} = \sum_{i=1}^{v_{\max}} \lambda_i J \left(\mu_{c,i} + (i-1) J^{-1}(I_A^{[V,D]}) \right) \quad (18)$$

where $\mu_{c,i}$ can be computed as

$$\mu_{c,i} = J^{-1} \left(f_D \left(J \left(i \cdot J^{-1}(I_A^{[V]}) \right), \frac{E_s}{N_0} \right) \right).$$

This leads to the overall EXIT characteristic of the combined variable node differential decoder

$$f_{V,D} \left(I, \frac{E_s}{N_0} \right) := \sum_{i=1}^{v_{\max}} \lambda_i J \left(J^{-1} \left(f_D \left(J \left(i \cdot J^{-1}(I) \right), \frac{E_s}{N_0} \right) \right) + (i-1) J^{-1}(I) \right)$$

which is a linear function in λ . Due to the linearity of $f_{V,D}(\cdot, \cdot)$, we can employ a simple linear programming optimization to find good values of λ_i for a given check node degree

Table 4: Theoretical thresholds values of E_s/N_0 (in dB) for the designed codes

	No constraint on L_2		$L_2 \leq 1 - r$	
	Full Interl.	Partial Interl.	Full Interl.	Partial Interl.
Gray Diff.	4.536	4.43	4.946	4.907
Natural Diff.	4.905	4.839	5.382	5.33

distribution, as described in [50]. However, if we only allow three different variable node degrees (and thus three partial interleavers), the problem reduces to a one-dimensional problem again, which we can solve in a similar way (using Algorithm 1) as for the case with full interleaving. However, we would like to point out that due to the linearity of $f_{V,D}(\cdot, \cdot)$, it is much easier to find *optimal* degree distributions. Numerical methods such as, e.g., differential evolution cannot guarantee to find the global optimum of the problem.

3.2.3 Comparison of Interleaving Schemes – Results

Using both interleaving schemes and differential QPSK transmission, we design degree distributions. We impose the constraint that the maximum variable node degree shall be $v_{\max} = 12$. For each interleaving scheme, we either use Gray differential encoding or natural differential encoding. For both options we have optimized codes using Algorithm 1 with variable degrees $\in \{2, 3, 12\}$ and regular check node degree. We additionally design codes for the constraint where $L_2 \leq 1 - r$. This constraint is necessary to avoid a high number of degree-2 nodes. It can be shown [62] that a potential error floor can occur if the fraction of degree-2 nodes is larger than $1 - r$. If we impose the constraint $L_2 \leq 1 - r$, then we can design a code that avoids—in the graph description—cycles containing only degree-2 nodes and with no information bits assigned to degree-2 nodes [63]. The condition $L_2 \leq 1 - r$ translates in the general case into

$$\lambda_2 \leq 2 \left(\frac{1}{r} - 1 \right) \sum_{j=3}^{v_{\max}} \frac{\lambda_j}{j},$$

which can be added to Algorithm 1.

We generate codes of target rate $r = \frac{4}{5} = 0.8$, a rate typically used in optical communications. A rate of $r = 0.8$ is a viable selection for current and future 100 Gbit/s (with QPSK) or 200 Gbit/s systems operating in a *dense wavelength division multiplex* (DWDM) setting with 50 GHz channel spacing and an exploitable bandwidth of roughly 37.5 GHz due to frequent filtering with non-flat frequency characteristic. The best possible achievable values of E_s/N_0 (corresponding to E_{best} in Algorithm 1) for the different code designs are shown in Tab. 4 and the degree distributions of the resulting codes are summarized in Tab. 5. We can see that Gray differential coding with partial interleaving leads to the best coded transmission schemes operating at the lowest possible E_s/N_0 values.

Figure 19 shows a first simulation results for the case of a QPSK modulation. We have constructed codes of size $n = 32000$ having the degree distributions from Tab. 5. The

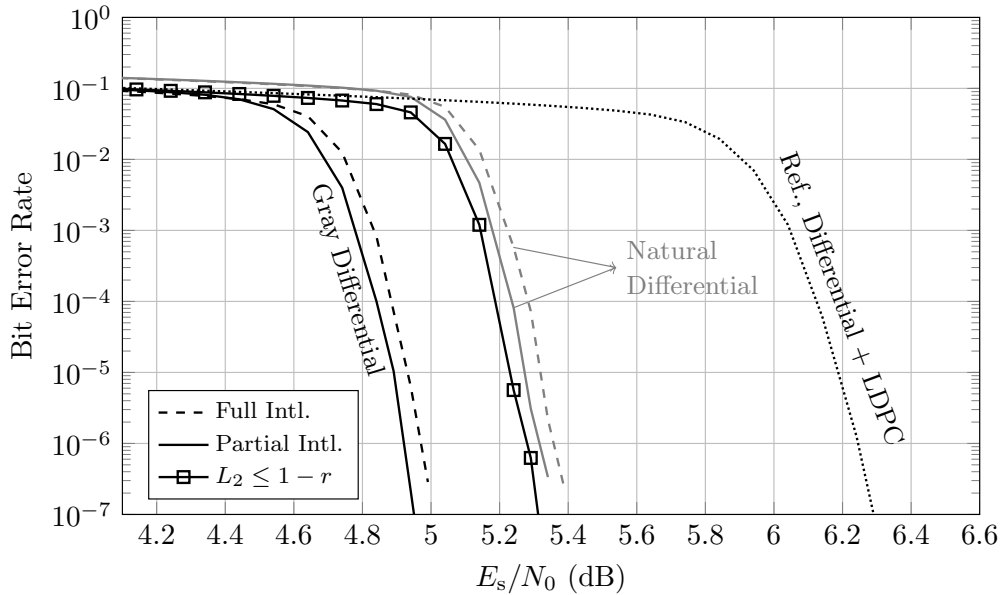


Figure 19: Simulation example, QPSK with $\gamma = 0$

utilized channel model is the phase-slip channel model from Fig. 3 with $\gamma = 0$. In this example, we wish to confirm the results of Tab. 4. As a reference scheme, we optimized an LDPC code for a simple AWGN channel with $v_{\max} = 12$ and regular check node degree $c_{\text{reg.}}$, which is used with *non-iterative* differential decoding. We can see that the results of Tab. 4 are indeed confirmed and the code with Gray differential coding and partial interleaving yields the best performance. As decoder, we use a conventional decoder as described in the Appendix of this chapter with 18 decoding iterations, where in each iteration, we invoke the differential decoder. Note that with the use of a layered decoder [64], the convergence speed can be increased and the same performance can be obtained by using only approximately 12 layered iterations. For this reason, the choice of 18 iterations is practical, as 12 layered LDPC iterations are deemed to be implementable [20].

Table 5: Degree distributions of all considered codes

Code	L_2	L_3	L_{12}	$c_{\text{reg.}}$
Gray diff., full intl.	0.959	0.002	0.039	12
Gray diff., partial intl.	0.919	0.002	0.079	14
Natural diff., full intl.	0.979	0.002	0.019	11
Natural diff., partial intl.	0.959	0.002	0.039	12
Gray diff., full intl., $L_2 \leq 1 - r$	0.198	0.78	0.022	15
Gray diff., partial intl., $L_2 \leq 1 - r$	0.198	0.78	0.022	15
Natural diff., full intl., $L_2 \leq 1 - r$	0.198	0.78	0.022	15
Natural diff., partial intl., $L_2 \leq 1 - r$	0.198	0.78	0.022	15

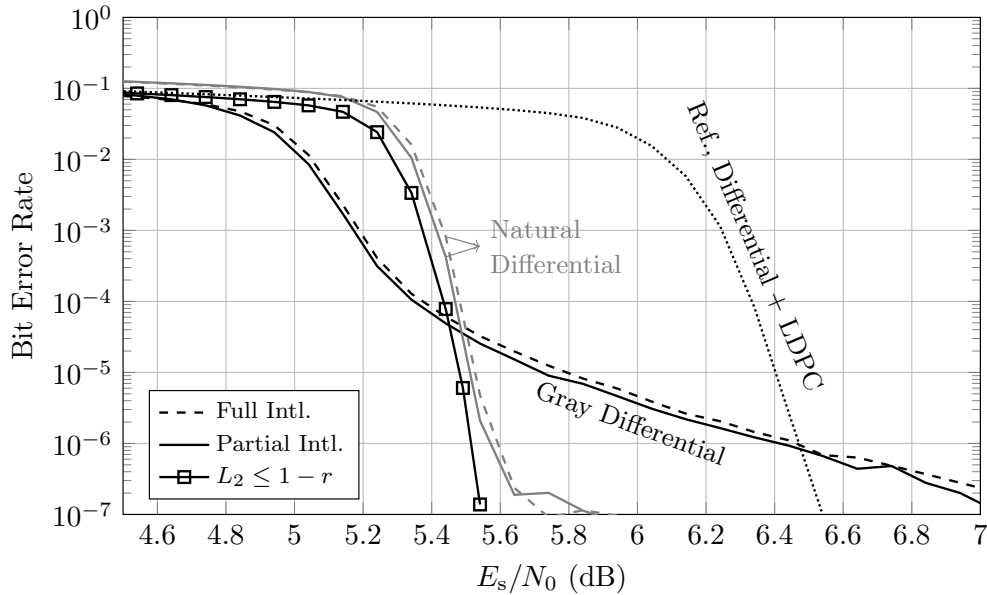


Figure 20: Simulation example, QPSK with $\gamma = 0.2$

In the second example, we increase the phase slip probability on the channel by choosing $\gamma = 0.2$. The simulation results for this case are shown in Fig. 20. We can observe that the formerly best case with Gray differential coding now shows a significant error floor. With natural differential coding, an error floor is observed as well, however, at several orders of magnitude smaller. This floor is mainly due to the large number of degree-2 nodes and the fact that $I_E^{[D]}(I_A^{[D]} = 1) < 1$ if $\gamma > 0$. Indeed, for this optimization, most of the variable nodes are of degree-2, i.e., λ_2 and consequently L_2 becomes very large. It has also been observed [56] that LDPC codes designed for differentially coded modulation require many degree-2 nodes. Degree-2 variable nodes are however a non-negligible contributor to the error floor, especially if there are cycles in the graph that connect only degree-2 variable nodes. It has been shown that cycles containing only degree-2 variable nodes can be avoided [62] if $\Lambda_2 \leq m = n(1 - r)$, i.e., if $L_2 \leq 1 - r$, which is why we have included that constraint into the optimization. In this case, we may design a systematic code and assign only parity bits to the degree-2 variable nodes. This further reduces the error floor as the bit error rate is calculated purely based on the systematic bits and the higher the variable node degree, the more reliable a bit is after decoding.

We have added the constraint $L_2 \leq 1 - r$ to the optimization routine and have found according degree distribution (summarized in Tab. 5). In the simulation results shown in Fig. 19, the performance of the code obtained with the $L_2 \leq 1 - r$ condition is shown by the curve with square markers for Gray differential coding. We see that in this case, we get a slightly better performance than natural differential coding, but have advantages regarding the residual bit error rate, at the expense of an increased required E_s/N_0 to allow

for successful decoding in the case where $\gamma = 0$ (see Fig. 19). Thus, depending on the required target bit error rate, we may either use the condition $L_2 \leq 1 - r$ or not. If an outer code is used that can correct up to an input bit error rate of $4.2 \cdot 10^{-3}$ (e.g., the staircase code [65]) we may use the code designed without the constraint on L_2 , but if we use a higher rate outer code as in [20, 63] that requires a very low input bit error rate, we may select the code designed with $L_2 \leq 1 - r$.

We can thus summarize that there are somewhat conflicting code design strategies. If $\gamma = 0$, we can use the code optimized for Gray differential coding with partial interleaving. This code will however lead to an elevated error floor if phase slips occur on the channel. This error floor has to be combated either with a properly designed outer code⁵ or by using only the code with the constraint $L_2 \leq 1 - r$, which however leads to a suboptimal performance in the phase-slip-free case ($\gamma = 0$). Another solution is the implementation of two codes, one for each case ($\gamma = 0$ and large γ). This latter method can guarantee best performance depending on the channel, but requires a feedback loop from the receiver to the transmitter, which may not be available in the network and of course it requires the implementation of two different codes, which may be too complex on an *application specific integrated circuit* (ASIC). In Sec. 4, we show a solution which requires only a single code and shows a more universal, channel-agnostic behavior.

3.3 Higher Order Modulation Formats with $V < Q$

In practical systems, we often have to deal with the case where $V < Q$, e.g., if 16-QAM is used, where we have $V = 4$ and $Q = 16$. In this case, we may use different techniques to optimize the code. We propose to refine the method of partial interleaving and to use only differential coding on a fraction of $\frac{\log_2 V}{\log_2 Q} = \frac{v}{q}$ of the bits. This is shown in Fig. 21. In this case, the value $\mu_{c,i}$ required in (18) is computed as

$$\mu_{c,i} = \frac{v}{q} J^{-1} \left(f_D \left(J \left(i \cdot J^{-1} (I_A^{[V]}) \right) \right) \right) + \left(1 - \frac{v}{q} \right) \bar{\mu}_c.$$

where $\bar{\mu}_c$ denotes the mean of the log-likelihood ratios of the bits that are not differentially encoded, obtained using a conventional bit-wise decoder [25] (see (25)) and averaged over all these bits. These bits correspond to the part of the constellation encoded with the rotationally invariant mapping (symbols within a region associated to a state S_i).

Besides this simple and direct approach, we can also use more involved methods, e.g., using the technique of *multi-edge-type* (MET) codes, as described in [50, 66, Ch. 7], but this is outside the scope of this chapter.

⁵Note that the implementation of a coding system with an outer cleanup code requires a thorough understanding of the LDPC code and a properly designed interleaver between the LDPC code and the outer code.

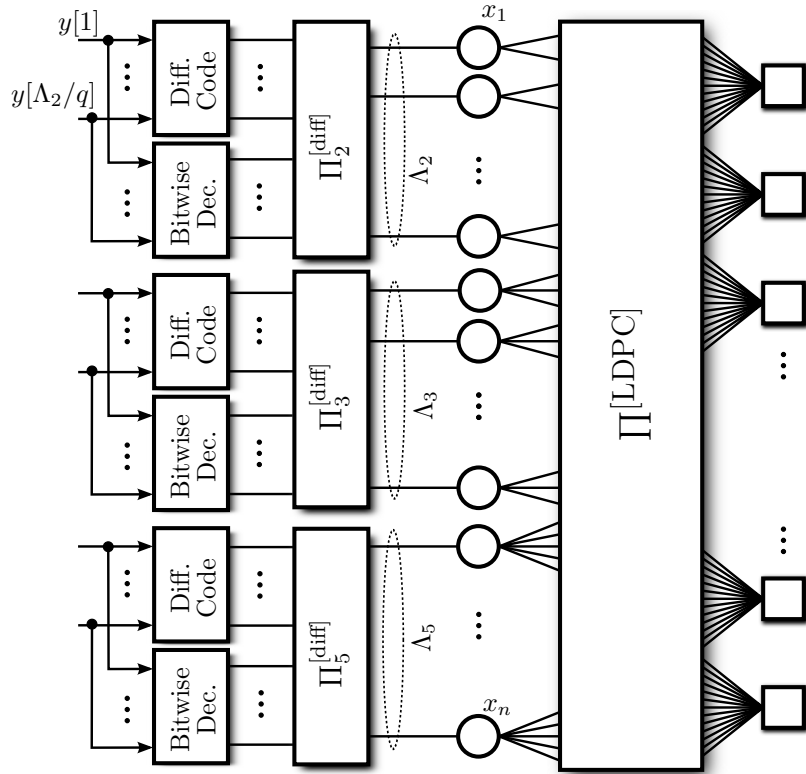


Figure 21: Schematic of the LDPC code with partial interleaving between LDPC code and differential decoder for the case where $V < Q$

4 Coded Differential Modulation with Spatially Coupled LDPC Codes

In the 1960s and the following decades, most coding research focused on block coding techniques, but many practical coding schemes were based upon convolutional codes [67]. With the advent of turbo codes [38], the rediscovery of LDPC codes, and advances in semiconductor technology, this suddenly changed so that today most new coding schemes are, again, block codes. The trend is, however, to return to convolutional-like structures [68] that can be efficiently encoded and decoded using sliding-window techniques.

In the last few years, the class of spatially coupled (SC) code ensembles has emerged [69, 70]. Spatially coupled codes were originally introduced more than a decade ago [71] and were then called *LDPC convolutional codes*. The appealing properties of SC codes were only recently noticed, when it was found that the performance of terminated SC-LDPC codes with simple belief propagation decoding approaches the *maximum a posteriori* (MAP) thresholds of the underlying ensemble [72, 73]. Thus, contrary to a common belief, introducing structure into LDPC codes leads to a class of (degenerated) realizations of LDPC codes

that demonstrate superior performance under belief propagation decoding. This effect of threshold saturation has been analyzed for the binary erasure channel (BEC) in [69] and it has been shown that spatially coupled LDPC codes can asymptotically achieve the MAP threshold of the underlying ensemble under belief propagation decoding. Recently, this result has been extended to more general channels and it has been shown in [70] that spatially coupled regular LDPC ensembles *universally* achieve capacity over binary-input memoryless output-symmetric channels: most codes in this ensemble are good for each channel realization in this class of channels.

Spatially coupled codes are now emerging in various applications. Two examples in the context of optical communications are the staircase code [65] and the braided BCH codes of [74], which are both rate $R = 239/255$ codes targeted for 100 GBit/s applications with hard-decision decoding. Both codes are spatially coupled BCH product codes that allow for a natural windowed decoder implementation. These codes can be interpreted as being generalized spatially coupled LDPC codes with variable node degree $d_v = 2$ and every bit participating in two BCH component codes, where the component BCH codes are able to correct up to 4 errors each. Another example is the IEEE 1901 power line communications standard, where an LDPC convolutional code is specified for the wavelet physical layer [75]. For a basic introduction to spatially coupled codes, we refer the interested reader to [51],[76].

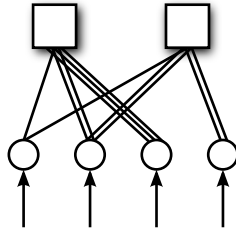
4.1 Protograph-Based Spatially Coupled LDPC Codes

In this chapter, we restrict ourselves to the class of protograph-based construction of SC-LDPC codes as introduced in, e.g., [72, 73, 77]. A protograph [78] is a convenient way of describing LDPC codes. Protograph codes are constructed from the P -cover of a relatively small graph which conveys the main properties of the code. In contrast to the graph representation of the LDPC code, the protograph may contain multiple edges. The code itself is constructed by placing P copies of the protograph next to each other (note that these have no interconnecting edges) and permuting the edges between the different copies of the protograph, such that the relation between the group of edges is respected. The construction of a small toy code is illustrated in Example 4.1.

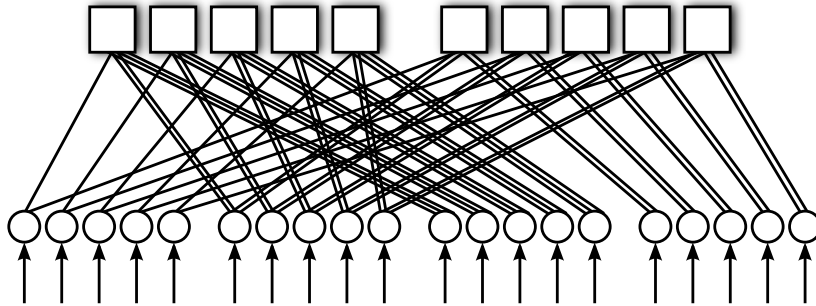
Example 4.1 *We illustrate the construction of larger codes based on protographs using a simple toy example. Starting with a prototype matrix, also called protomatrix*

$$\mathbf{B} = \begin{pmatrix} 1 & 2 & 3 & 0 \\ 1 & 2 & 0 & 2 \end{pmatrix}$$

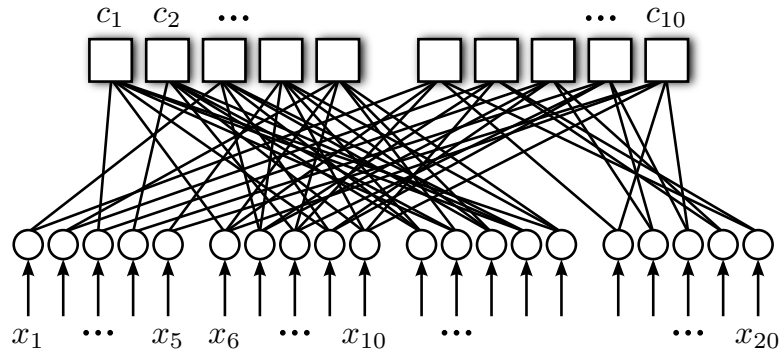
we show how a P -cover is constructed. First, we construct an equivalent graph of the base matrix in the same way as we constructed the graph of the LDPC code in Sec. 3.1.2. The difference is that the non-zero entries in \mathbf{B} indicate the number of parallel edges connecting the variables with the checks. The graph representation of the protomatrix \mathbf{B} is given by:



In the next step, we construct the P -cover of this graph, which means that we simply place P copies of this graph next to each other:



This graph is still not a valid LDPC code as it contains parallel edges and the P sub-graphs are not connected. In order to remove the parallel edges and to construct a more randomized code, we permute in a next step all edges that are within one edge group, i.e., that correspond to a single entry $B_{i,j}$ of \mathbf{B} . This permutation is performed in such a way that no parallel edges persist. The final code graph is then obtained by



Note that it is not possible to draw this code with a single interleaver $\Pi^{[LDPC]}$ as the code in Fig. 16, because it is actually a multi-edge-type ensemble [50, Sec. 7.1] and for every single entry $B_{i,j}$ of \mathbf{B} , an individual interleaver is required. The parity-check matrix \mathbf{H} can be constructed from \mathbf{B} by replacing each entry $B_{i,j}$ (row i , column j) of \mathbf{B} by the superposition of $B_{i,j}$ permutation matrices⁶, chosen such that no two “1”s are in the same

⁶A permutation matrix \mathbf{P} is a square binary matrix (i.e., a matrix containing only “0” and “1”) where each row contains exactly one “1” and where each column contains exactly one “1”.

One can say that the convergence of spatially coupled codes is well understood meanwhile. A thorough analysis for the binary erasure channel is given in [69] and extended to general binary input memoryless channels in [70]. The convergence behavior of the iterative decoder can be subdivided into two convergence regions

- the region of *macro-convergence*, where convergence is dominated by the code’s degree distribution and convergence prediction by conventional EXIT charts is possible.
- the region of *micro-convergence*, where the convergence is dominated by spatial coupling and termination effects.

The region of *macro-convergence* is observed in the first decoding iterations and at high channel SNRs. On the other hand, the region of *micro-convergence* is observed at low SNRs close to the thresholds of the code. In the region of micro-convergence, the decoding process can be visualized as a decoding wave [80] that slowly progresses through the graph from the boundaries onward. This wave-like behavior allows the efficient design of windowed decoders [81] where the decoding window follows the decoding wave. The understanding of the dynamics of the decoding wave, especially its speed [82], are essential for designing high-performing codes and effective windowed decoders.

4.2 Spatially Coupled LDPC Codes with Iterative Demodulation

In this section, we combine spatially coupled codes with a differential decoder and use common analysis techniques to show how the detector front-end influences the performance of the codes. As we have seen, in conventional LDPC code design, usually the code needs to be “matched” to the transfer curve of the detection front-end. If the code is not well matched to the front-end, a performance loss occurs. If the detector front-end has highly varying characteristics, due to, e.g., varying channels or varying phase slip probabilities, several codes need to be implemented and always the right code needs to be chosen for maximum performance, which appears impractical in optical networks where a feedback channel from the receiver to the transmitter can potentially be difficult to realize.

On the other hand, in contrast to a random ensemble of the same degree profile, spatially coupled LDPC codes can converge below the pinch-off in the EXIT chart, so even if the code is not well matched to the differential decoder we can hope to successfully decode due to the micro-convergence effect. So, even with a varying channel and detector characteristics, we can use a single code which is *universally* good in all scenarios. This means that the code design can stay *agnostic* to the channel/detector behavior.

We determine the thresholds of the protograph-based spatially coupled codes combined with demodulation and detection by an extension of the PEXIT technique [83] with the Gaussian approximation of the check node operation [84]. A refined version of the PEXIT technique taking into account the windowed decoder of spatially coupled codes has been presented in [85]. The mutual information analysis used for the design of degree distributions in LDPC codes has to be modified slightly to account for the protograph structure. Instead of analyzing and tracking a single mutual information value I , we now have to track an

individual mutual information value for each non-zero entry at row i and column j of the protomatrix $\mathbf{B}^{[\text{conv}]}$. We denote the respective outgoing (incoming) edge mutual information by $I_{E,i,j}^{[V,D]}$ ($I_{A,i,j}^{[V,D]}$) or by $I_{E,i,j}^{[C]}$ ($I_{A,i,j}^{[C]}$), depending if the message is computed by the combined variable node detector engine (“ V, D ”) or by the check node engine (“ C ”). Note that we assume that the messages are Gaussian distributed and can be described by a single parameter, their mean μ (with the variance 2μ , see [19] and [50] for details).

As in the previous section, we assume that the demodulator/detector properties can be described by means of an EXIT characteristic [53, 27] which we denote by $f_D(\cdot, \cdot)$. If the message at the input of the detector is Gaussian distributed with mean μ , then the detector output mean for (protograph) variable j is obtained by

$$\mu_{c,j} = J^{-1} \left(f_D \left(J \left(\sum_{i=1}^{(L+m_s)m'} B_{i,j}^{[\text{conv}]} J^{-1}(I_{A,i,j}^{[V,D]}) \right), \frac{E_s}{N_0} \right) \right) \quad (20)$$

leading to the combined variable node and detector update characteristic

$$I_{E,i,j}^{[V,D]} = J \left(\mu_{c,j} + (B_{i,j}^{[\text{conv}]} - 1) J^{-1} \left(I_{A,i,j}^{[V,D]} \right) + \sum_{\substack{k=1 \\ k \neq i}}^{(L+m_s)m'} B_{k,j}^{[\text{conv}]} J^{-1} \left(I_{A,k,j}^{[V,D]} \right) \right), \quad (21)$$

which has to be evaluated for all $(i, j) \in [1, \dots, (L+m_s)m'] \times [1, \dots, Ln']$ where $B_{i,j}^{[\text{conv}]} \neq 0$. The check node information is computed according to [84]

$$I_{E,i,j}^{[C]} = J \left(\phi^{-1} \left(1 - \left[1 - \phi \left(J^{-1}(I_{A,i,j}^{[C]}) \right) \right]^{B_{i,j}^{[\text{conv}]} - 1} \prod_{\substack{k=1 \\ k \neq j}}^{Ln'} \left[1 - \phi \left(J^{-1}(I_{A,i,k}^{[C]}) \right) \right]^{B_{i,k}^{[\text{conv}]}} \right) \right). \quad (22)$$

which again has to be evaluated for all combinations of (i, j) such that $B_{i,j}^{[\text{conv}]} \neq 0$. The function $\phi(\mu)$, which is used to compute the evolution of the mean of the Gaussian messages in the check node update is given by

$$\phi(x) = \begin{cases} 1 - \frac{1}{\sqrt{4\pi x}} \int_{-\infty}^{\infty} \tanh\left(\frac{u}{2}\right) \exp\left(-\frac{(u-x)^2}{4x}\right) du, & \text{if } x > 0 \\ 1, & \text{if } x = 0 \end{cases} \quad (23)$$

Numerical approximations for (23) and its inverse function are given in [84].

The evaluation of the information is carried out in an iterative way: First, we initialize the process by setting $I_{A,i,j}^{[V,D]}(1) = 0$ for all possible (i, j) where the “(1)” denotes the first iteration. Using (20), we first compute $\mu_{c,j}(1)$, $\forall j \in [1, Ln']$ and use $\mu_{c,j}(1)$ to compute $I_{E,i,j}^{[V,D]}(1)$ by evaluating (21) for all $(i, j) \in [1, \dots, (L+m_s)m'] \times [1, \dots, Ln']$. We then set

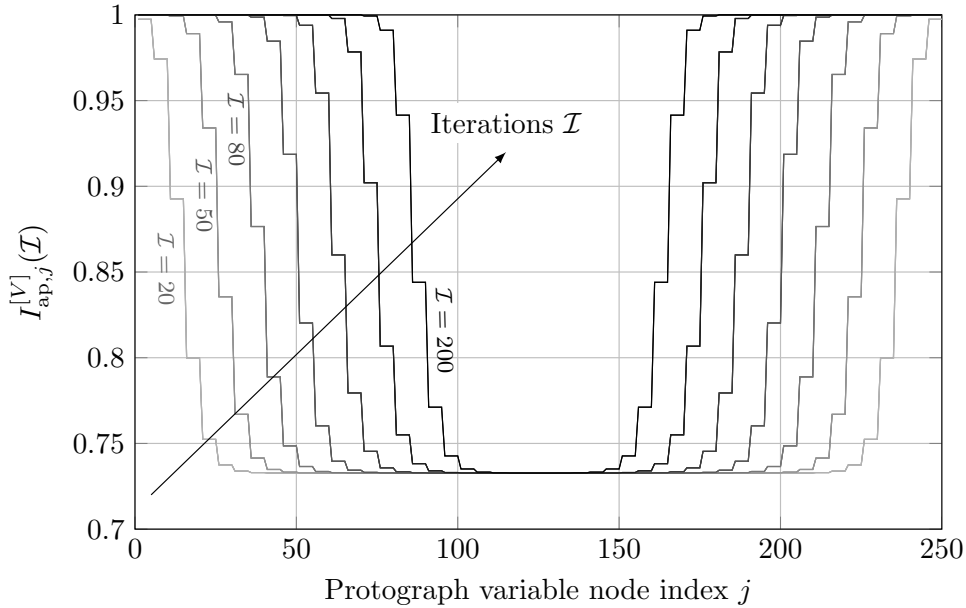


Figure 22: Wave-like decoding behavior of the spatially coupled, protograph-based LDPC code ($L = 50$) with Gray differential coding and $\gamma = 0.2$ for $E_s/N_0 = 4.8$ dB

$I_{A,i,j}^{[C]}(1) = I_{E,i,j}^{[V,D]}(1)$ and evaluate (22) yielding $I_{E,i,j}^{[C]}(1)$. By setting $I_{A,i,j}^{[V,D]}(2) = I_{E,i,j}^{[C]}(1)$ we may proceed to the second iteration and compute $\mu_{c,j}(2)$, $I_{E,i,j}^{[V,D]}(2)$ and $I_{E,i,j}^{[C]}(2)$ in this sequence. Finally, after \mathcal{I} iterations, we may—for each variable node in the protograph—determine the *a posteriori* reliability by

$$I_{\text{ap},j}^{[V]} = J \left(\mu_{c,j} + \sum_{k=1}^{(L+m_s)m'} B_{k,j}^{[\text{conv}]} J^{-1} \left(I_{A,k,j}^{[V,D]}(\mathcal{I}) \right) \right).$$

We illustrate the behavior of $I_{\text{ap},j}^{[V]}$, which gives an indication of the reliability of the P bits that will be assigned to position j in the protograph by means of an example. We consider a spatially coupled code of rate $r = 0.8$ with $m_s = 2$ and with $\mathbf{B}_0 = \mathbf{B}_1 = \mathbf{B}_2 = (1 \ 1 \ 1 \ 1 \ 1)$. We use QPSK with Gray differential coding and set $\gamma = 0.2$ at $E_s/N_0 = 4.8$ dB, i.e., according to (3), phase slips occur on the channel with a probability $P_{\text{slip}} \approx 0.0082$. Figure 22 shows the behavior of the *a posteriori* mutual information $I_{\text{ap},j}^{[V]}(\mathcal{I})$ as a function of the decoding iterations \mathcal{I} . We can see that the mutual information increases in a wave-like way. Starting from the boundaries of the codeword, the mutual information converges towards 1 with an increasing number of iterations from the outside towards the inside until both waves meet and the whole codeword has been successfully decoded.

4.3 Windowed Differential Decoding of SC-LDPC Codes

By observing the wave-like decoding behavior [80] in Fig. 22, we note that only parts of the protograph get updated when carrying out iterations. For instance, the reliability of the protograph variable node indices 110 to 140 stay at an almost constant value during the first 200 iterations. Likewise, the protograph variable node indices 1 to 30 have already converged to 1 after 110 iterations and do not benefit anymore from additional decoding iterations. This wave-like behavior thus leads to an efficient *windowed decoder* [81, 86], which follows the decoding wave and only carries out operations on the part of the protograph that benefits from further decoding iterations. The windowed decoder works in principle as an LDPC decoder, just with the difference that it operates on a fraction of the parity-check matrix. The windowed decoder is characterized by a window length w and operates on a portion of the protomatrix containing w vertically stacked copies of \mathbf{B}_r

$$\tilde{\mathbf{B}}^{[\text{conv}]} = \begin{pmatrix} \mathbf{B}_{m_s} & \cdots & \mathbf{B}_0 & & \\ & \mathbf{B}_{m_s} & \cdots & \mathbf{B}_0 & \\ & & \ddots & \cdots & \ddots \\ & & & \mathbf{B}_{m_s} & \cdots & \mathbf{B}_0 \end{pmatrix}_{wm' \times (w+m_s)n'} \quad (24)$$

The decoder takes a block of $(w + m_s)n'$ protograph variables (i.e., $(w + m_s)Pn'$ code bits), and carries out \mathcal{I}_w decoding iterations on this block (using the conventional decoding scheme described in the Appendix). After having carried out \mathcal{I}_w iterations, the window is shifted by n' protograph variables (Pn' code bits) and the left-most portion of Pn' code bits are considered to be decoded. Then the process starts again. At the beginning of the process, the decoding window is initialized with perfect knowledge of the boundary values. For details, we refer the interested reader to [81] and [87].

4.4 Design of Protograph-Based SC-LDPC Codes for Differential Coded Modulation

We show by means of an example how to construct good protographs for SC-LDPC codes in the context of differential coded modulation [88]. For simplicity, we restrict ourselves to SC-LDPC codes with $m_s = 2$ leading to a protomatrix given by

$$\mathbf{B}_c = \begin{pmatrix} \mathbf{B}_0 & & & & \\ \mathbf{B}_1 & \mathbf{B}_0 & & & \\ \mathbf{B}_2 & \mathbf{B}_1 & \cdots & & \\ & \mathbf{B}_2 & \cdots & \mathbf{B}_0 & \\ & & \cdots & \mathbf{B}_1 & \\ & & & & \mathbf{B}_2 \end{pmatrix}.$$

We select $m_s = 2$, as this choice leads to windowed decoders with a relatively compact decoding window. Note that the minimum required decoding window size grows almost

linearly with m_s . Another viable choice would be $m_s = 1$, however, simulation results which are not shown here have indicated that a better performance can be expected with $m_s = 2$.

We consider iterative differential decoding as described in the previous section using the modified slip-resilient BCJR algorithm based on the trellis of Fig. 10 and wish to design coding schemes of rate $r = 0.8$ (25% OH). We use protographs leading to regular SC-LDPC codes with variable degree $v_{\text{reg.}} = 3$ and check degree $c_{\text{reg.}} = 15$. The reason for using regular codes is that it has been shown in [69] that regular SC-LDPC are sufficient to achieve capacity and this particular code has a MAP threshold very close to capacity. Furthermore, due to the regularity, the implementation of the decoder can be simplified and the error floor is expected to be very low (increasing $v_{\text{reg.}}$ further may even lead to lower error floors).

Although $v_{\text{reg.}}$, $c_{\text{reg.}}$ and m_s are fixed, we still need to find good protomatrices \mathbf{B}_0 , \mathbf{B}_1 and \mathbf{B}_2 . In order to have a very simple structure, we fix $m' = 1$ and $n' = 5$, leading to the smallest possible protomatrices. We have constructed all 1837 possible such combinations of protographs (unique up to column permutation) and computed decoding thresholds for all these protographs using the above described method. We selected the protographs with the 50 best thresholds and carried out Monte Carlo simulations with three different windowed decoders:

- The first setup uses a window size of $w = 4$ and carries out $\mathcal{I}_w = 3$ iterations per decoding step.
- ◇ The second setup uses a window size of $w = 7$ and carries out $\mathcal{I}_w = 2$ iterations per decoding step.
- △ The third setup uses a window size of $w = 16$ and carries out a single iteration per decoding step, i.e., $\mathcal{I}_w = 1$.

Note that with all three setups, every coded bit undergoes an equivalent number of 18 iterations, leading to the same complexity of all decoders and the same complexity as the LDPC coded schemes presented in Sec. 3. Further note that the number of differential decoder executions per coded bit amounts $w + m_s$ and thus depends on the setup. In the case of LDPC coded differential demodulation, we have executed the differential decoder for each iteration. The required E_s/N_0 (in dB) to achieve a target BER of 10^{-6} for the 50 selected protographs is shown in Fig. 23 for $L = 100$ and $P_{\text{slip}} \in \{0, 0.01\}$. Based on the results of Fig. 23, we select the protograph with index 3 which has the best performance compromise at $P_{\text{slip}} = 0$ and $P_{\text{slip}} = 0.01$, and which is given by $\mathbf{B}_0 = (1 \ 1 \ 1 \ 1 \ 1)$, $\mathbf{B}_1 = (1 \ 0 \ 0 \ 0 \ 0)$, and $\mathbf{B}_2 = (1 \ 2 \ 2 \ 2 \ 2)$.

Finally, we use this protograph to construct a code by first lifting the protographs \mathbf{B}_i with $P = 40$ and using the intermediate result in a second step to generate a *quasi-cyclic* (QC) code with circulant permutation matrices of size 50×50 . The resulting parity-check submatrices \mathbf{H}_i associated to \mathbf{B}_i have size $\dim \mathbf{H}_i = 2000 \times 10000$. As reference, we use QPSK with Gray differential coding and pick the two best codes found in Sec. 3.2: partial

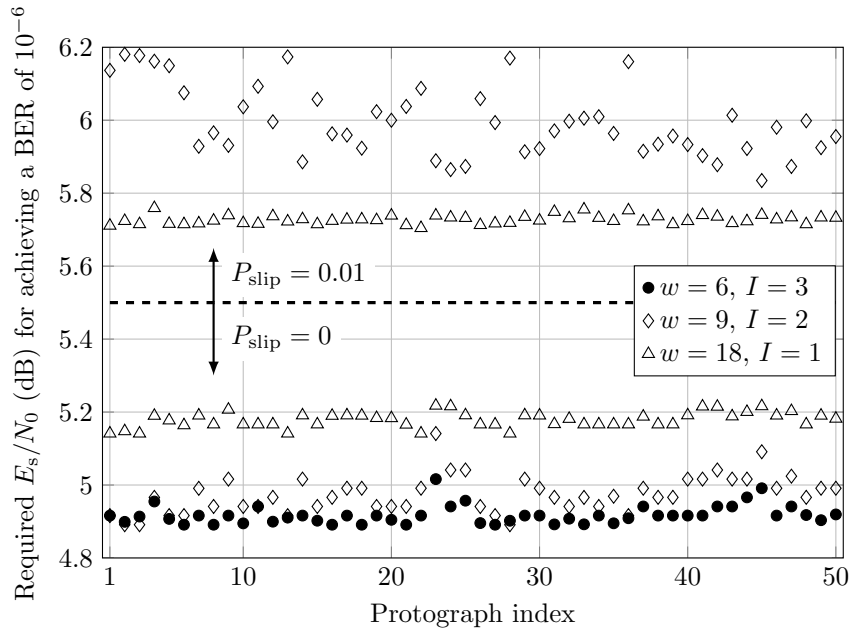


Figure 23: Required E_s/N_0 for 50 different protographs

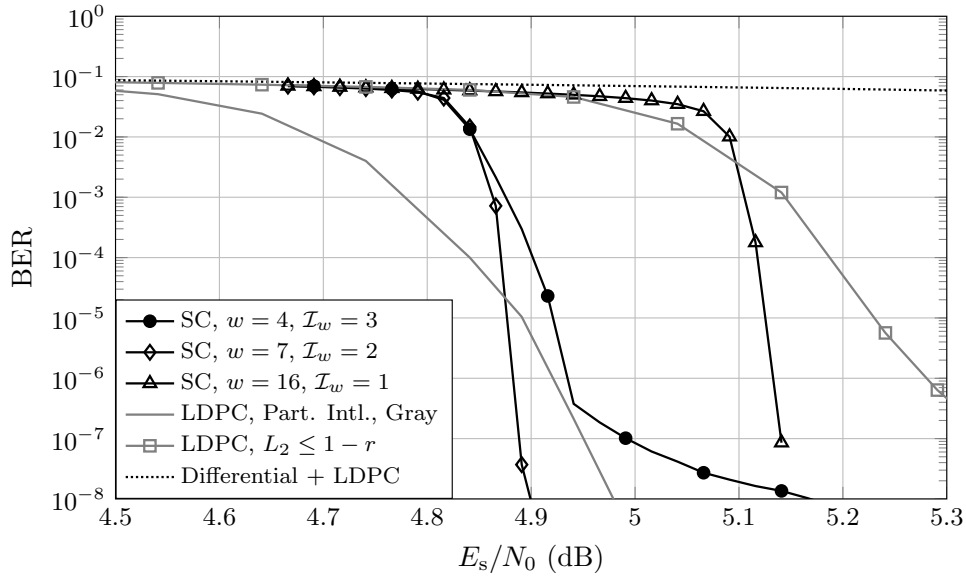


Figure 24: Simulation results of proposed and reference schemes for QPSK with $\gamma = 0$

interleaving with no restriction on L_2 and partial interleaving with $L_2 \leq 1 - r$. As in Figs. 19 and 20, we use $I = 18$ decoding iterations in all cases. The results are shown in Fig. 24 for $\gamma = 0$ (i.e., no phase slips) and in Fig. 25 for $\gamma = 0.2$.

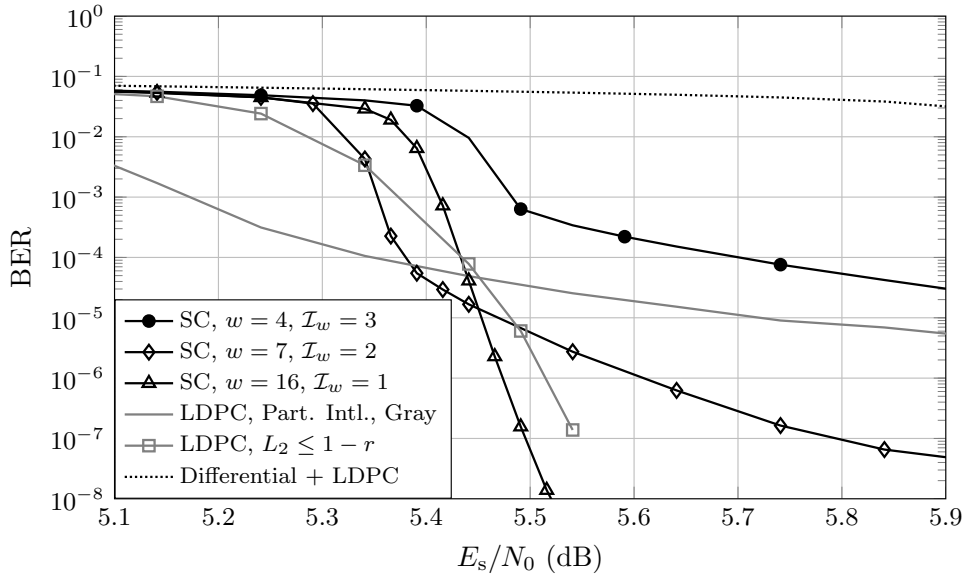


Figure 25: Simulation results of proposed and reference schemes for QPSK with $\gamma = 0.2$

We can see from the results that for $\gamma = 0$, the LDPC code with partial interleaving (no restriction on L_2) already yields a very good performance within 1 dB of the theoretically minimum E_s/N_0 , while the code with the constraint on L_2 entails a performance loss of about 0.4 dB (see also Figs. 19 and 20). The SC-LDPC code with the second decoder setup ($w = 7$) outperforms the LDPC code for low BERs due to the steepness of the waterfall curve. If the phase slip probability is nonzero with $\gamma = 0.2$, which may occur in a highly nonlinear DWDM transmission with OOK neighbors, we observe from Fig. 19 and Fig. 25 that the LDPC code no longer performs well and has a severe error floor requiring strong outer coding. The error floor can be reduced by designing a code with $L_2 \leq 1 - r$. If $\gamma = 0.2$, the SC-LDPC code with decoder setup 3 almost shows the same performance as the LDPC code with the constraint $L_2 \leq 1 - r$ and outperforms it at low error rates (we did not observe any error floor in our simulations).

The proposed SC-LDPC code has the important advantage of *universality* [77]: A single SC code is powerful in all transmission scenarios requiring only a single *channel agnostic transmitter* and a receiver selecting the best decoding setup depending on γ and P_{slip} . The transmission scheme can thus be kept simple and only a *single* code needs to be implemented. In the setup with conventional LDPC codes, two different codes have to be implemented, depending on the setup: one code for small γ and another code, possibly with $L_2 \leq 1 - r$, for larger values of γ . The transmitter has to know the expected γ on the channel and adapt the coding scheme accordingly, which requires an undesired feedback channel and changes in the network control plane. Another possibility is to deliberately design an LDPC code which shall perform well in both cases [56]: this leads however to a compromise in the construction and codes which are not able to compete with codes optimized for

a specific scenario. With the SC-LDPC code, we can use a single code and use receiver processing to estimate γ and setup the windowed decoder (w and \mathcal{I}_w) accordingly. Note that for large γ , it is advantageous to use a long window w , which means that the number of differential decoding executions per bit shall be maximized. This is in contrast to the HTDD approach [20], which however uses a differential decoder not adapted to the channel. We conclude that executing the differential detector doesn't degrade the performance as long as it is well adapted to the channel model.

5 Conclusions

In this chapter, we have described some important aspects of soft-decision forward error correction with iterative decoding. We have shown that the phenomenon of phase slips, which occurs frequently in the case of coherent long-haul optical communications, can be combated effectively using iterative differential decoding. We have shown that the achievable information rate is not affected by iterative differential decoding and that differential decoding only leads to an unavoidable performance loss if not properly decoded. We have further shown how phase slips affect the achievable rate and how to design a trellis diagram describing the differential code affected by phase slips. In order to achieve the best possible performance, this differential decoder needs some well-adapted code design. We have proposed different design guidelines for LDPC codes and have shown that, depending on the channel quality, there is a different code design which may lead to the desired performance, especially if very low residual bit error rates are targeted. Finally, we have shown that spatially coupled codes offer a more universal code design and lead to codes that are more agnostic to the channel and thus enable the implementation of a single code that performs equally well in all channel conditions and that even outperforms conventional LDPC codes.

A LDPC Coded Differential Modulation – Decoding Algorithms

The decoders we consider (which can include simplified versions like binary message passing decoders [89]) rely on the knowledge of the channel⁷. The communication channel, or an equivalent communication channel comprising the physical channel as well as various inner receiver and signal processing stages, can be characterized by its *conditional probability* $P(z|y)$, i.e., the probability of observing z at the receiver assuming a transmitted modulation symbol $y \in \mathcal{M}$. Note that we restrict ourselves to memoryless channels, which can be achieved in practice by sufficiently long interleaving of the channel input. Notable examples

⁷In optical coherent receivers, either channel models like the AWGN channel are assumed together or histogram based methods may be employed [12, Sec. 6.2]. Sometimes, the worst case channel for which the system is designed may be assumed.

are the *binary symmetric channel* (BSC) with ($y = x$)

$$\begin{aligned} P(z = 0|x = 0) &= 1 - \epsilon & P(z = 1|x = 0) &= \epsilon \\ P(z = 0|x = 1) &= \epsilon & P(z = 1|x = 1) &= 1 - \epsilon \end{aligned}$$

which is frequently used to model the hard-decision channel. Another famous example is the real-valued *additive white Gaussian noise* (AWGN) channel with *binary phase shift keying* (BPSK) modulation with $y = (-1)^x$ and (real-valued) noise variance $\sigma_n^2 = N_0/2$, leading to

$$p(z|y) = \frac{1}{\sqrt{\pi N_0}} \exp\left(-\frac{(z-y)^2}{N_0}\right).$$

As the computation with probabilities tends to be numerically unstable and hinders potential hardware implementations, frequently *log-likelihood ratios* (LLRs) [90] are employed. The LLR $L(z[t])$ for received symbol $z[t]$ at time instant t is defined for BPSK as

$$L(z[t]) = \log \frac{p(z[t]|x[t] = 0)}{p(z[t]|x[t] = 1)},$$

where $\log(\cdot)$ is the natural logarithm. It turns out that for the AWGN channel with BPSK modulation, we have

$$L_{\text{AWGN}}(z[t]) = \frac{2}{\sigma_n^2} z[t] = 4 \frac{E_s}{N_0} z[t] = 4r \frac{E_b}{N_0} z[t] =: L_c \cdot z[t].$$

This last equation means that the LLR $L_{\text{AWGN}}(z[t])$ is obtained by multiplication of $z[t]$ with a constant $L_c := \frac{2}{\sigma_n^2}$, which depends on the noise variance only. Usually, the noise variance is assumed to be constant and the constant L_c is predetermined and set to a value suitable for implementation. The noise variance may also be estimated at the receiver [91].

If higher order modulation formats based on a constellation \mathcal{M} are employed, we have to use a more involved computation rule. Starting from the mapping function $\phi(\mathbf{b})$, we first define the i th inverse mapping function

$$\phi_i^{-1}(b) = \left\{ \tilde{\mathbf{y}} = \phi(\tilde{b}_1, \dots, \tilde{b}_{i-1}, b, \tilde{b}_{i+1}, \dots, \tilde{b}_q) : \tilde{\mathbf{y}} \in \mathcal{M}, (\tilde{b}_1, \dots, \tilde{b}_{i-1}, \tilde{b}_{i+1}, \dots, \tilde{b}_q) \in \mathbb{F}_2^{q-1} \right\}$$

Thus, $\phi_i^{-1}(b)$ returns the set of all modulation symbols to which a bit pattern whereof the i th bit takes on the value b , is assigned. The LLR for the ubiquitous *bit-wise* decoder [25] is then given by

$$L(b_i[t]) = \log \left(\frac{\sum_{\tilde{\mathbf{y}} \in \phi_i^{-1}(0)} p(z[t]|\tilde{\mathbf{y}})}{\sum_{\tilde{\mathbf{y}} \in \phi_i^{-1}(1)} p(z[t]|\tilde{\mathbf{y}})} \right). \quad (25)$$

Before we step ahead and describe the decoding algorithms, we first introduce the \max^* operation, which simplifies the description of the BCJR decoder [92]

Definition 4 *The max* operation. The max* operations is defined as*

$$\max^*(\delta_1, \delta_2) := \max(\delta_1, \delta_2) + \log\left(1 + e^{-|\delta_1 - \delta_2|}\right) = \log\left(e^{\delta_1} + e^{\delta_2}\right)$$

and can be conveniently approximated by

$$\max^*(\delta_1, \delta_2) \approx \max(\delta_1, \delta_2).$$

The max* operation has several properties, namely

$$\begin{aligned}\max^*(\delta_1, \delta_2) &= \max^*(\delta_2, \delta_1) \\ \lim_{\delta_1 \rightarrow -\infty} \max^*(\delta_1, \delta_2) &= \delta_2 \\ \max^*(\delta_1, \delta_2, \delta_3) &= \max^*(\delta_1, \max^*(\delta_2, \delta_3))\end{aligned}$$

The latter property allows us to define

$$\max_{j=1}^{\chi} \delta_j = \max^*(\delta_1, \delta_2, \dots, \delta_\chi) = \max^*(\delta_1, \max^*(\delta_2, \dots \max^*(\delta_{\chi-1}, \delta_\chi) \dots))$$

and with the trivial case

$$\max_{j=1}^1 \delta_j = \delta_1.$$

Differential Decoding

The soft-input soft-output differential decoding is carried out using the BCJR algorithm [6]. We just summarize the operations of the BCJR algorithm in the LLR domain, such that it can be immediately applied. We give the equations for the case $V = 4$, which we have used in our simulations in this chapter. We use the trellis diagram of Fig. 10 to describe the BCJR algorithm. The algorithm consists of computing a forward and a backward recursion. In the forward recursion, the variables $\tilde{\alpha}_t(\mathbf{S}_i)$ are updated for $i \in \{1, 2, 3, 4\}$. The initialization, which describes the initial differential memory, is usually carried out as

$$\begin{aligned}\tilde{\alpha}_0(\mathbf{S}_1) &= 0 \\ \tilde{\alpha}_0(\mathbf{S}_i) &= -\infty \quad \text{for } i \in \{2, 3, 4\}.\end{aligned}$$

The recursive update is given by (for all $j \in \{1, 2, 3, 4\}$)

$$\tilde{\alpha}_t(\mathbf{S}_j) = \max_{i=1}^4 \max_{s=0}^3 \left(\tilde{\alpha}_{t-1}(\mathbf{S}_i) + \tilde{\gamma}_t(i, j, s) \right)$$

Similarly, the backward recursion is carried out with the initialization $\tilde{\beta}_{\tilde{n}}(\mathbf{S}_j) = 0$, for $j \in \{1, 2, 3, 4\}$, where \tilde{n} denotes the length of the sequence of modulation symbols to be decoded. We have

$$\tilde{\beta}_{t-1}(\mathbf{S}_i) = \max_{j=1}^4 \max_{s=0}^3 \left(\tilde{\beta}_t(\mathbf{S}_j) + \tilde{\gamma}_t(i, j, s) \right)$$

Before giving the equation to compute $\gamma(i, j, s)$, we first introduce the sets $\mathcal{M}_{S_i} \subset \mathcal{M}$ which contain all modulation symbols that are associated to state S_i (that are within the region associated with state S_i). For the example of the QPSK constellation of Fig. 4, $\mathcal{M}_{S_1} = \left\{ \frac{1+i}{\sqrt{2}} \right\}$ and for the example of the 16-QAM constellation of Fig. 5, we have

$$\mathcal{M}_{S_1} = \left\{ \frac{1+i1}{\sqrt{10}}, \frac{3+i1}{\sqrt{10}}, \frac{1+i3}{\sqrt{10}}, \frac{3+i3}{\sqrt{10}} \right\}.$$

The variable $\tilde{\gamma}_t(i, j, \zeta)$ describes the (logarithmic) probability of a state transition from state S_i at time $t-1$ to state S_j at time t provided that the phase slip occurrence descriptor $s[t]$ takes on the value ζ . We have

$$\begin{aligned} \tilde{\gamma}_t(i, j, \zeta) &= \frac{1}{N_0} \sum_{\chi \in \mathcal{M}_{S_j}} |z[t] - \chi|^2 + \frac{1}{2} \sum_{\kappa=1}^v \left(1 - 2\check{f}_{\text{diff},\kappa}^{-1}(S_i, S_j, s) \right) L_{(t-1)v+\kappa}^{\text{[apriori,II]}} + \\ &+ \log P(s = \zeta). \end{aligned}$$

Note that with the phase slip model introduced in Sec. 2.2, we may abbreviate $\log P(s = \zeta) = |\zeta| \log \xi$. The function $\check{f}_{\text{diff},\kappa}^{-1}(S_i, S_j, s)$ returns the κ th bit b_κ of the differential encoding map that causes a state transition from S_i to $S_{j'}$, where j' is an intermediate state leading to the final state $j = ((j' + s - 1) \bmod V) + 1$ after taking into account the phase slip. $L_i^{\text{[apriori,II]}}$ contains the input LLR values $L_i^{\text{[apriori]}}$ that are provided by the LDPC decoder after full or partial interleaving. In the initial execution (first iteration) of the differential decoder, we may set $L_i^{\text{[apriori,II]}} = 0$.

Finally, we obtain for each $t \in \{1, \dots, \tilde{n}\}$ and $\kappa \in \{1, \dots, v\}$

$$\begin{aligned} L_{(t-1)v+\kappa}^{\text{[diff,II]}} &= \max_{\substack{(i,j,s) \\ \check{f}_{\text{diff},\kappa}^{-1}(S_i, S_j, s)=0}}^* \left(\tilde{\alpha}_{t-1}(S_i) + \tilde{\gamma}_t(i, j, s) + \tilde{\beta}_t(S_j) \right) - \\ &- \max_{\substack{(i,j,s) \\ \check{f}_{\text{diff},\kappa}^{-1}(S_i, S_j, s)=1}}^* \left(\tilde{\alpha}_{t-1}(S_i) + \tilde{\gamma}_t(i, j, s) + \tilde{\beta}_t(S_j) \right) - L_{(t-1)v+\kappa}^{\text{[apriori,II]}}. \end{aligned}$$

After (partial or full) deinterleaving of $L_i^{\text{[diff,II]}}$, we obtain $L_i^{\text{[diff]}}$ which is used as input of the LDPC decoder.

LDPC decoding

A vast collection of various decoding algorithms for LDPC codes exist and we refer to the broad body of literature for a good introduction (see, e.g., [18, 93]). Most of these decoders are message passing decoders, where the most prominent is probably the sum-product decoder [18]. In what follows, we describe the sum-product decoder and the closely related min-sum decoder, which can be interpreted as being an approximation of the sum-product decoder.

In order to describe the sum-product and min-sum decoders, we introduce the set $\mathcal{N}(m) := \{j : H_{m,j} \neq 0\}$ which contains the positions (columns) of non-zero entries at row m of the parity-check matrix \mathbf{H} . For the matrix given in Example 3.1, we have $\mathcal{N}(1) = \{1; 4; 11; 12; 15; 22; 24; 25; 28; 29; 30; 31\}$. Similarly, the set $\mathcal{M}(n) := \{i : H_{i,n} \neq 0\}$ contains the positions (rows) of non-zero entries at column n of the parity-check matrix \mathbf{H} . Again, for the exemplary matrix of Example 3.1, we have $\mathcal{M}(1) = \{1; 2\}$, $\mathcal{M}(2) = \{3; 5\}$ and so on.

Within the sum-product decoder, messages are exchanged between the variable nodes and the check nodes, thus the name *message passing decoder*. We denote the message that is passed from variable node i towards check node j by $L_{i,j}^{[v \rightarrow c]}$. Similarly, the message that is passed from check node j towards variable node i is denoted by $L_{i,j}^{[v \leftarrow c]}$. Before first executing the LDPC decoder with a new frame of data, all messages are set to zero, i.e., $L_{i,j}^{[v \rightarrow c]} = L_{i,j}^{[v \leftarrow c]} = 0$ for all combinations of $(j, i) \in [1, \dots, m] \times [1, \dots, n]$ such that $H_{j,i} \neq 0$.

The sum-product LDPC coder computes for each of the n variables, i.e., for each transmitted bits, the total sum

$$L_i^{[\text{tot}]} = L_i^{[\text{diff}]} + \sum_{j \in \mathcal{M}(i)} L_{i,j}^{[v \leftarrow c]}, \quad \forall i \in \{1, \dots, n\}$$

Using this total sum, the variable-to-check messages may be computed as

$$L_{i,j}^{[v \rightarrow c]} = L_i^{[\text{tot}]} - L_{i,j}^{[v \leftarrow c]}, \quad \forall i \in \{1, \dots, n\}, \forall j \in \mathcal{M}(i)$$

In the second step, the check node update rule is carried out to compute new check-to-variable messages

$$L_{i,j}^{[v \leftarrow c]} = 2 \tanh^{-1} \left(\prod_{i' \in \mathcal{N}(j) \setminus \{i\}} \tanh \left(\frac{L_{i',j}^{[v \rightarrow c]}}{2} \right) \right), \forall j \in \{1, \dots, m\} \forall i \in \mathcal{N}(j)$$

where the inner product is taken over all entries in $\mathcal{N}(j)$ except the one under consideration i . This is indicated by the notation $\mathcal{N}(j) \setminus \{i\}$. Usually, in practical implementations, simplified approximations to this update rule are implemented, for example the scaled min-sum rule [94]

$$L_{i,j}^{[v \leftarrow c]} = \nu \left(\prod_{i' \in \mathcal{N}(j) \setminus \{i\}} \text{sign} \left(L_{i',j}^{[v \rightarrow c]} \right) \right) \min_{i' \in \mathcal{N}(j) \setminus \{i\}} |L_{i',j}^{[v \rightarrow c]}|$$

where ν is an appropriately chosen scaling factor. See [95] for other simplified variants of the sum-product algorithm.

With the updated check-to-variable node messages, a new *a priori* message that is transmitted to the differential decoder may be computed as

$$L_i^{[\text{apriori}]} = \sum_{j \in \mathcal{M}(i)} L_{i,j}^{[v \leftarrow c]}, \quad \forall i \in \{1, \dots, n\}.$$

Note that the convergence of the sum-product decoder as described here can be considerably improved by using the so-called row-layered decoder [64], which allows to roughly halve the number of decoding iterations. Many additional possible decoder variants, which may be better suited for an ASIC implementation than the message passing decoder described here, are discussed in [18].

References

- [1] W. Grover, “Error correction in dispersion-limited lightwave systems,” *Journal of Lightwave Technology*, vol. 6, pp. 643–654, 1988.
- [2] C. Fludger, D. Nuss, and T. Kupfer, “Cycle-slips in 100G DP-QPSK transmission systems,” in *Proc. OFC/NFOEC*, 2012. Paper OTu2G.1.
- [3] M. Y. Leong, K. J. Larsen, G. Jacobsen, S. Popov, D. Zibar, and S. Sergeyev, “Dimensioning BCH codes for coherent DQPSK systems with laser phase noise and cycle slips,” *J. Lightw. Technol.*, vol. 32, no. 21, pp. 3446–3450, 2014.
- [4] T. Pfau, “Carrier recovery algorithms and real-time DSP implementation for coherent receivers,” in *Proc. OFC*, Mar. 2014. Paper W4K.1.
- [5] P. Hoeher and J. Lodge, ““Turbo DQPSK”: Iterative differential PSK demodulation and channel decoding,” *IEEE Trans. Commun.*, vol. 47, pp. 837–843, June 1999.
- [6] L. Bahl, J. Cocke, F. Jelinek, and J. Raviv, “Optimal decoding of linear codes for minimizing symbol error rate,” *IEEE Trans. Inf. Theory*, vol. 20, pp. 284–287, Mar. 1974.
- [7] L. Schmalen, “Energy efficient FEC for optical transmission systems,” in *Proc. Optical Fiber Communications Conference (OFC)*, (San Francisco, CA, USA), Mar. 2014.
- [8] H. Bülow, X. Lu, and L. Schmalen, “Experimental analysis of transmission and soft decoding of optimized 4D constellations,” in *Asia Communications and Photonics Conference (ACP)*, (Beijing, China), 2013.
- [9] R. Koetter, A. C. Singer, and M. Tüchler, “Turbo equalization,” *IEEE Signal Process. Mag.*, vol. 21, pp. 67–80, Jan. 2004.
- [10] T. Fujimori, T. Koike-Akino, T. Sugihara, K. Kubo, K. Koguchi, T. Mizuochi, C. Ohshima, H. Nakashima, and T. Hoshida, “A study on the effectiveness of turbo equalization with FEC for nonlinearity compensation in coherent WDM transmissions,” in *Proc. OptoElectronics and Communications Conference (OECC)*, June 2013.
- [11] L. Beygi, E. Agrell, J. Kahn, and M. Karlsson, “Coded modulation for fiber-optic networks,” *IEEE Signal Process. Mag.*, vol. 31, pp. 93–103, Mar. 2014.

- [12] I. B. Djordjevic, W. Ryan, and B. Vasic, *Coding for Optical Channels*. Springer, 2010.
- [13] T. Koike-Akino, K. Kojima, D. S. Millar, K. Parsons, Y. Miyata, W. Matsumoto, T. Sugihara, and T. Mizuoichi, "Cycle slip-mitigating turbo demodulation in LDPC-coded coherent optical communications," in *Proc. OFC*, 2014. Paper M3A.3.
- [14] W. Weber, "Differential encoding for multiple amplitude and phase shift keying systems," *IEEE Commun. Lett.*, vol. 26, pp. 385–391, Mar. 1978.
- [15] T. Pfau, S. Hoffmann, and R. Noe, "Hardware-efficient coherent digital receiver concept with feedforward carrier recovery for M -QAM constellations," *J. Lightw. Technol.*, vol. 27, pp. 989–999, Apr. 2009.
- [16] A. Bisplinghoff, S. Langenbach, T. Kupfer, and B. Schmauss, "Turbo differential decoding failure for a coherent phase slip channel," in *Proc. European Conference on Optical Communications (ECOC)*, Sept. 2012. Paper Mo.1.A.5.
- [17] A. Leven and S. ten Brink, "Method of decoding optical data signals." European Patent Application EP2506516, Oct. 2012.
- [18] W. E. Ryan and S. Lin, *Channel Codes: Classical and Modern*. Cambridge University Press, 2009.
- [19] S. ten Brink, "Convergence behavior of iteratively decoded parallel concatenated codes," *IEEE Trans. Commun.*, vol. 49, pp. 1727–1737, Oct. 2001.
- [20] A. Bisplinghoff, S. Langenbach, N. Beck, C. Fludger, and C. Schulien, "Cycle slip tolerant hybrid turbo differential decoding," in *Proc. European Conference on Optical Communications (ECOC)*, (Cannes, France), Sept. 2014. Paper Th.2.3.3.
- [21] C. E. Shannon, "A mathematical theory of communication," *The Bell System Technical Journal*, vol. 27, pp. 379–423, 623–656, July and October 1948.
- [22] T. M. Cover and J. A. Thomas, *Elements of Information Theory*. John Wiley & Sons, Inc., 2006.
- [23] G. D. Forney, Jr., "Trellis shaping," *IEEE Trans. Inf. Theory*, vol. 38, pp. 281–300, Mar. 1992.
- [24] B. P. Smith and F. R. Kschischang, "A pragmatic coded modulation scheme for high-spectral-efficiency fiber-optic communications," *J. Lightw. Technol.*, vol. 30, pp. 2047–2053, July 2012.
- [25] A. Guillén i Fàbregas, A. Martinez, and G. Caire, "Bit-interleaved coded modulation," *Found. Trends Commun. Inf. Theory*, vol. 5, pp. 1–153, Jan. 2008.

- [26] S. ten Brink, “Exploiting the chain rule of mutual information for the design of iterative decoding schemes,” in *Allerton Annual Conference on Communication, Control and Computing*, (Monticello, IL, USA), Oct. 2001.
- [27] A. Ashikhmin, G. Kramer, and S. ten Brink, “Extrinsic information transfer functions: model and erasure channel properties,” *IEEE Trans. Inf. Theory*, vol. 50, pp. 2657–2673, Nov. 2004.
- [28] M. Franceschini, G. Ferrari, R. Raheli, and A. Curtoni, “Serial concatenation of LDPC codes and differential modulations,” *IEEE J. Sel. Areas Commun.*, vol. 23, pp. 1758–1768, Sept. 2005.
- [29] G. Caire, G. Taricco, and E. Biglieri, “Bit-interleaved coded modulation,” *IEEE Trans. Inf. Theory*, vol. 44, pp. 927–946, May 1998.
- [30] S. ten Brink, J. Speidel, and R.-H. Yan, “Iterative demapping and decoding for multi-level modulation,” in *Proc. GLOBECOM*, (Sydney), 1998.
- [31] X. Li and J. A. Ritcey, “Bit-interleaved coded modulation with iterative decoding,” in *IEEE International Conference on Communications (ICC)*, (Vancouver, BC, Canada), June 1999.
- [32] F. Yu, N. Stojanovic, F. Hauske, D. Chang, Z. Xiao, G. Bauch, D. Pflüger, C. Xie, Y. Zhao, L. Jin, Y. Li, L. Li, X. Xu, and Q. Xiong, “Soft decision LDPC turbo decoding for DQPSK modulation in coherent optical receivers,” in *Proc. ECOC*, (Geneva, CH), Sept. 2011. Paper We.10.P1.70.
- [33] L. Schmalen, “Low-complexity phase slip tolerant LDPC-based FEC scheme,” in *Proc. ECOC*, (Cannes, France), Sept. 2014. Paper Th.2.3.2.
- [34] L. Schmalen, “A low-complexity LDPC coding scheme for channels with phase slips,” *J. Lightw. Technol.*, vol. 33, no. 7, pp. 1319–1325, 2015.
- [35] S. Bellini, M. Ferrari, A. Tomasoni, C. Costantini, L. Razzetti, and G. Gavioli, “LDPC design for block differential modulation in optical communications,” *J. Lightw. Technol.*, vol. 33, no. 1, pp. 78–88, 2015.
- [36] L. Hanzo, T. H. Liew, and B. L. Yeap, *Turbo Coding, Turbo Equalisation and Space-Time Coding for Transmission over Fading Channels*. John Wiley & Sons, Ltd., 2002.
- [37] R. G. Gallager, *Low-Density Parity-Check Codes*. Cambridge, MA, USA: M.I.T. Press, 1963.
- [38] C. Berrou, A. Glavieux, and P. Thitimajshima, “Near Shannon limit error-correcting coding and decoding: Turbo-codes (1),” in *IEEE International Conference on Communications (ICC)*, pp. 1064–1070, May 1993.

- [39] D. C. MacKay and R. Neal, “Near Shannon limit performance of low density parity check codes,” *Electron. Letters*, vol. 32, pp. 1645–1646, 1996.
- [40] M. Luby, M. Mitzenmacher, A. Shokrollahi, D. A. Spielman, and V. Stemann, “Practical loss-resilient codes,” in *Proc. ACM Symposium on Theory of Computing*, pp. 150–159, 1997.
- [41] IEEE, “802.11, wireless LAN medium access control (MAC) and physical layer (PHY) specifications,” 2012.
- [42] ETSI, “DVB-S2, ETSI standard EN 302 307 v.1.2.1,” 2009.
- [43] IEEE, “802.3an, local and metropolitan area networks-specific requirements part 3: Carrier sense multiple access with collision detection (CSMA/CD): Access method and physical layer specifications,” 2006.
- [44] Y. Miyata, K. Kubo, H. Yoshida, and T. Mizuochi, “Proposal for frame structure of optical channel transport unit employing LDPC codes for 100 Gb/s FEC,” in *Proc. OFC/NFOEC, paper NThB2*, 2009.
- [45] T. Richardson, “Error floors of LDPC codes,” in *Proc. Allerton Conference on Communications, Control and Computing*, 2003.
- [46] L. Dolecek, P. Lee, Z. Zhang, V. Anantharam, B. Nikolic, and M. Wainwright, “Predicting error floors of structured LDPC codes: Deterministic bounds and estimates,” *IEEE J. Sel. Areas Commun.*, vol. 27, pp. 908–917, Aug. 2009.
- [47] D. A. Morero, C. M. A, F. A. Ramos, T. A. Goette, O. E. Agazzi, and M. R. Hueda, “Non-concatenated FEC codes for ultra-high speed optical transport networks,” in *Proc. GLOBECOM*, pp. 1–5, 2011.
- [48] N. Bonello, S. Chen, and L. Hanzo, “Design of low-density parity-check codes,” *IEEE Vehicular Technology Magazine*, vol. 6, no. 4, 2011.
- [49] G. Liva, S. Song, L. Lan, Y. Zhang, S. Lin, and W. Ryan, “Design of LDPC codes: A survey and new results,” *Journal of Communication Software and Systems*, vol. 2, no. 3, pp. 191–211, 2006.
- [50] T. Richardson and R. Urbanke, *Modern Coding Theory*. Cambridge University Press, 2008.
- [51] A. Leven and L. Schmalen, “Status and recent advances on forward error correction technologies for lightwave systems,” *J. Lightw. Technol.*, vol. 32, pp. 2735–2750, Aug. 2014.
- [52] T. J. Richardson, M. A. Shokrollahi, and R. L. Urbanke, “Design of capacity-approaching irregular low-density parity-check codes,” *IEEE Trans. Inf. Theory*, vol. 47, pp. 619–637, Feb. 2001.

- [53] S. ten Brink, G. Kramer, and A. Ashikhmin, “Design of low-density parity-check codes for modulation and detection,” *IEEE Trans. Commun.*, vol. 52, no. 4, pp. 670–678, 2004.
- [54] F. Schreckenbach, “Iterative decoding of bit-interleaved coded modulation,” tech. rep., PhD thesis, TU Munich, Munich, Germany, 2007.
- [55] E. Sharon, A. Ashikhmin, and S. Litsyn, “Analysis of low-density parity-check codes based on EXIT functions,” *IEEE Trans. Commun.*, vol. 54, pp. 1407–1414, Aug. 2006.
- [56] D. Pflüger, G. Bauch, F. Hauske, and Y. Zhao, “Design of LDPC codes for hybrid 10 Gbps/100 Gbps optical systems with optional differential modulation,” in *Proc. ITG SCC*, 2013.
- [57] D. Pflüger, G. Bauch, Y. Zhao, and F. N. Hauske, “Conditions on degree distributions to compensate differential penalty by LDPC turbo decoding,” in *Proc. IEEE VTC*, 2013.
- [58] K. V. Price, R. Storn, and J. A. Lampinen, eds., *Differential Evolution – A Practical Approach to Global Optimization*, ch. 7.7, “Design of efficient erasure codes with differential evolution” by A. Shokrollahi and R. Storn. Springer, 2005.
- [59] G. Lechner, J. Sayir, and I. Land, “Optimization of LDPC codes for receiver frontends,” in *Proc. ISIT*, (Seattle, WA), 2006.
- [60] B. Benammar, N. Thomas, C. Pouillat, M. Boucheret, and M. Dervin, “Asymptotic analysis and design of iterative receivers for non linear ISI channels,” in *Proc. International Symposium on Turbo Codes & Iterative Information Processing*, (Bremen, Germany), Aug. 2014.
- [61] A. Alvarado, L. Szczecinski, E. Agrell, and A. Svensson, “On BICM-ID with multiple interleavers,” *IEEE Commun. Lett.*, vol. 14, pp. 785–787, Sept. 2010.
- [62] J. Tillich and G. Zemor, “On the minimum distance of structured LDPC codes with two variable nodes of degree 2 per parity-check equation,” in *Proc. IEEE ISIT*, (Seattle, WA, USA), pp. 1549–1553, July 2006.
- [63] K. Sugihara, Y. Miyata, T. Sugihara, K. Kubo, H. Yoshida, W. Matsumoto, and T. Mizuochi, “A spatially-coupled type LDPC code with an NCG of 12 dB for optical transmission beyond 100 Gb/s,” in *Proc. OFC*, 2013. Paper OM2B.4.
- [64] D. Hocevar, “A reduced complexity decoder architecture via layered decoding of LDPC codes,” in *Proc. IEEE Workshop on Signal Processing Systems (SiPS)*, 2004.
- [65] B. P. Smith, A. Farhood, A. Hunt, F. R. Kschischang, and J. Lodge, “Staircase codes: FEC for 100 Gb/s OTN,” *J. Lightw. Technol.*, vol. 30, no. 1, pp. 110–117, 2012.

- [66] L. Zhang and F. R. Kschischang, “Multi-edge-type low-density parity-check codes for bandwidth-efficient modulation,” *IEEE Trans. Commun.*, vol. 61, pp. 43–52, Jan. 2013.
- [67] D. J. Costello, Jr. and G. D. Forney, Jr., “Channel coding: The road to channel capacity,” *Proc. IEEE*, vol. 95, no. 6, pp. 1150–1177, 2007.
- [68] M. Tavares, *On Low-Density Parity-Check Convolutional Codes: Constructions, Analysis and VLSI Implementations*. PhD thesis, TU Dresden, Dresden, Germany, 2010.
- [69] S. Kudekar, T. Richardson, and R. Urbanke, “Threshold saturation via spatial coupling: Why convolutional LDPC ensembles perform so well over the BEC,” *IEEE Trans. Inf. Theory*, vol. 57, pp. 803–834, Feb. 2011.
- [70] S. Kudekar, T. Richardson, and R. Urbanke, “Spatially coupled ensembles universally achieve capacity under belief propagation,” *IEEE Trans. Inf. Theory*, 2013.
- [71] A. J. Felström and K. S. Zigangirov, “Time-varying periodic convolutional codes with low-density parity-check matrix,” *IEEE Trans. Inf. Theory*, vol. 45, pp. 2181–2191, June 1999.
- [72] M. Lentmaier, G. P. Fettweis, K. S. Zigangirov, and D. J. Costello, Jr., “Approaching capacity with asymptotically regular LDPC codes,” in *Proc. Information Theory and Applications Workshop (ITA)*, Feb 2009.
- [73] M. Lentmaier, D. G. M. Mitchell, G. Fettweis, and D. J. Costello, Jr., “Asymptotically good LDPC convolutional codes with AWGN channel thresholds close to the Shannon limit,” in *Proc. Intern. Sympo. on Turbo Codes & Iterative Information Proc. (ISTC)*, (Brest, France), Sept. 2010.
- [74] Y.-Y. Jian, H. D. Pfister, K. R. Narayanan, R. Rao, and R. Mazareh, “Iterative hard-decision decoding of braided BCH codes for high-speed optical communication,” in *Proc. GLOBECOM*, (Atlanta, GA, USA), pp. 2398–2403, Dec. 2013.
- [75] IEEE, “IEEE standard for broadband over power line networks: Medium access control and physical layer specifications,” tech. rep., Std. 1901, 2010.
- [76] D. J. Costello, Jr., L. Dolecek, T. E. Fuja, J. Kliewer, D. G. M. Mitchell, and R. Smerandache, “Spatially coupled sparse codes on graphs: theory and practice,” *IEEE Commun. Mag.*, vol. 52, pp. 168–176, July 2014.
- [77] L. Schmalen and S. ten Brink, “Combining spatially coupled LDPC codes with modulation and detection,” in *Proc. ITG SCC*, (Munich, Germany), Jan. 2013.
- [78] J. Thorpe, “Low-Density Parity-Check (LDPC) codes constructed from protographs,” tech. rep., IPN Progress Report 42-154, 2003.

- [79] D. G. M. Mitchell, M. Lentmaier, and D. J. Costello, Jr., “AWGN channel analysis of terminated LDPC convolutional codes,” in *Proc. Information Theory and Applications Workshop (ITA)*, 2011.
- [80] S. Kudekar, T. Richardson, and R. Urbanke, “Wave-like solutions of general one-dimensional spatially coupled systems,” tech. rep., CoRR, arXiv:1208:5273, 2012.
- [81] A. R. Iyengar, P. H. Siegel, R. Urbanke, and J. K. Wolf, “Windowed decoding of spatially coupled codes,” in *Proc. ISIT*, July 2011.
- [82] V. Aref, L. Schmalen, and S. ten Brink, “On the convergence speed of spatially coupled LDPC ensembles,” in *Proc. Allerton Conference on Communications, Control, and Computing*, Oct. 2013. arXiv:1307.3780.
- [83] G. Liva and M. Chiani, “Protograph LDPC codes design based on EXIT analysis,” in *Proc. of GLOBECOM*, 2007.
- [84] S. Chung, T. J. Richardson, and R. L. Urbanke, “Analysis of sum-product decoding of low-density parity-check codes using a Gaussian approximation,” *IEEE Trans. Inf. Theory*, vol. 47, pp. 657–670, Feb. 2001.
- [85] C. Häger, A. Graell i Amat, F. Brännström, A. Alvarado, and E. Agrell, “Improving soft FEC performance for higher-order modulations via optimized bit channel mappings,” *Optics Express*, vol. 22, pp. 14544–14558, June 2014.
- [86] M. Lentmaier, M. M. Prenda, and G. Fettweis, “Efficient message passing scheduling for terminated LDPC convolutional codes,” in *Proc. ISIT*, (St. Petersburg, Russia), 2011.
- [87] A. R. Iyengar, M. Papaleo, P. H. Siegel, J. K. Wolf, A. Vanelli-Coralli, and G. E. Corazza, “Windowed decoding of protograph-based LDPC convolutional codes over erasure channels,” *IEEE Trans. Inf. Theory*, vol. 58, pp. 2303–2320, Apr. 2012.
- [88] L. Schmalen, S. ten Brink, and A. Leven, “Spatially-coupled LDPC protograph codes for universal phase slip-tolerant differential decoding,” in *Proc. OFC*, (Los Angeles, CA, USA), 2015.
- [89] G. Lechner, T. Pedersen, and G. Kramer, “Analysis and design of binary message passing decoders,” *IEEE Trans. Commun.*, vol. 60, pp. 601–607, Mar. 2012.
- [90] J. Hagenauer, E. Offer, and L. Papke, “Iterative decoding of binary block and convolutional codes,” *IEEE Trans. Inf. Theory*, vol. 42, pp. 429–445, Mar. 1996.
- [91] C. F. Mecklenbräuker and S. Paul, “On estimating the signal to noise ratio from BPSK signals,” in *Proc. ICASSP*, (Philadelphia, PA, USA), Mar. 2005.

- [92] P. Robertson, E. Villebrun, and P. Hoeher, “A comparison of optimal and sub-optimal MAP decoding algorithms operating in the log domain,” in *IEEE International Conference on Communications (ICC)*, (Seattle, WA, USA), pp. 1009–1013, June 1995.
- [93] T. K. Moon, *Error Correction Coding - Mathematical Methods and Algorithms*. John Wiley & Sons, Inc., 2005.
- [94] J. Chen and M. P. C. Fossorier, “Near optimum universal belief propagation based decoding of low-density parity check codes,” *IEEE Trans. Commun.*, vol. 50, pp. 406–414, Mar. 2002.
- [95] J. Zhao, F. Zarkeshvari, and A. H. Banihashemi, “On implementation of min-sum algorithm and its modifications for decoding low-density parity-check (LDPC) codes,” *IEEE Trans. Commun.*, vol. 53, pp. 549–554, Apr. 2005.